

Old Brains Come Uncoupled in Sleep: Slow Wave-Spindle Synchrony, Brain Atrophy, and Forgetting

Highlights

- Precise coupling of NREM slow waves and spindles dictates memory consolidation
- Aging impairs slow wave-spindle coupling, leading to overnight forgetting
- Age-related atrophy in mPFC predicts the failure of such coupling and thus memory

Authors

Randolph F. Helfrich, Bryce A. Mander, William J. Jagust, Robert T. Knight, Matthew P. Walker

Correspondence

rhelfrich@berkeley.edu

In Brief

Helfrich et al. demonstrate that the precise coupling between sleeping brainwaves, called slow waves and spindles, supports memory retention. However, this brainwave coupling during sleep is impaired in older adults due to loss of tissue in the medial frontal lobe, resulting in next-day forgetting.

Old Brains Come Uncoupled in Sleep: Slow Wave-Spindle Synchrony, Brain Atrophy, and Forgetting

Randolph F. Helfrich,^{1,2,6,*} Bryce A. Mander,^{3,4} William J. Jagust,^{1,4} Robert T. Knight,^{1,4,5} and Matthew P. Walker^{1,4,5}

¹Helen Wills Neuroscience Institute, UC Berkeley, 132 Barker Hall, Berkeley, CA 94720, USA

²Department of Psychology, University of Oslo, Forskningsveien 3A, 0373 Oslo, Norway

³Department of Psychiatry and Human Behavior, UC Irvine, 101 The City Dr., Orange, CA 92868, USA

⁴Department of Psychology, UC Berkeley, Tolman Hall, Berkeley, CA 94720, USA

⁵These authors contributed equally

⁶Lead Contact

*Correspondence: rhelfrich@berkeley.edu

<https://doi.org/10.1016/j.neuron.2017.11.020>

SUMMARY

The coupled interaction between slow-wave oscillations and sleep spindles during non-rapid-eye-movement (NREM) sleep has been proposed to support memory consolidation. However, little evidence in humans supports this theory. Moreover, whether such dynamic coupling is impaired as a consequence of brain aging in later life, contributing to cognitive and memory decline, is unknown. Combining electroencephalography (EEG), structural MRI, and sleep-dependent memory assessment, we addressed these questions in cognitively normal young and older adults. Directional cross-frequency coupling analyses demonstrated that the slow wave governs a precise temporal coordination of sleep spindles, the quality of which predicts overnight memory retention. Moreover, selective atrophy within the medial frontal cortex in older adults predicted a temporal dispersion of this slow wave-spindle coupling, impairing overnight memory consolidation and leading to forgetting. Prefrontal-dependent deficits in the spatiotemporal coordination of NREM sleep oscillations therefore represent one pathway explaining age-related memory decline.

INTRODUCTION

The precise temporal coordination of non-rapid-eye-movement (NREM) sleep oscillations has been proposed to support the long-term consolidation of memory (Diekmann and Born, 2010; Walker and Stickgold, 2006). Within these theoretical frameworks, temporal interactions between cortical slow oscillations (SOs; <1.25 Hz), sleep spindles (~12–16 Hz), and hippocampal ripples (~80–100 Hz) form a hierarchy that allows for information transformation necessary for long-term memory retention (Diekmann and Born, 2010; Frankland and Bontempi,

2005; Latchoumane et al., 2017; Rasch and Born, 2013; Staresina et al., 2015). In particular, the depolarizing “up-states” of the SOs are proposed to facilitate sleep spindle and ripple expression, with hippocampal ripples being temporally nested into spindle troughs (Rasch and Born, 2013; Staresina et al., 2015). The coupling of these NREM oscillations is thought to support intrinsically timed information transfer across several spatiotemporal scales underlying long-term memory (Diekmann and Born, 2010).

There is, however, limited empirical evidence supporting this oscillatory interaction model of hippocampal memory consolidation. Non-invasive brain stimulation findings have demonstrated that boosting SO power can indirectly co-modulate sleep spindle activity (Ladenbauer et al., 2017; Marshall et al., 2006), while SO-spindle coupling during a nap in young adults tracks offline memory retention (Niknazar et al., 2015). Yet, the mechanistic relationship of SO-spindle synchrony and how this determines the success or failure of overnight hippocampal-dependent memory consolidation remains unknown, as does the causal necessity of brain regions in supporting coupled NREM oscillation dynamics and memory benefit.

Regarding the latter, there is growing evidence that aging markedly disrupts sleep and overnight memory consolidation (Mander et al., 2017). If sleep oscillatory coupling is compromised in older adults, what is it about the aging brain that degrades interactive synchrony of NREM oscillations, thereby leading to memory impairment? This question is of special relevance as it may reveal a currently under-appreciated mechanism (impaired SO-spindle coupling) that contributes to memory decline in later life and, if identified, would define a novel therapeutic target for clinical intervention (Ladenbauer et al., 2017).

Here, we address these unanswered questions by combining structural MRI, polysomnography with full-head (19 channel) scalp electroencephalography (EEG), and the assessment of sleep-dependent hippocampal memory in young and older adults. We specifically tested the hypothesis that the precise temporal coupling of cortical NREM SOs and spindles, as predicted by theoretical models, facilitates overnight memory retention in young adults and whether older adults have a temporal uncoupling of these oscillations, leading to impaired overnight

memory. Moreover, based on evidence in young and older adults demonstrating that the structural gray matter (GM) morphology of the medial prefrontal cortex (mPFC) is associated with the quality of SO (Mander et al., 2013; Saletin et al., 2013), and that this same mPFC region is an EEG source generator of SO linked to spindles (Murphy et al., 2009), we further tested the hypothesis that structural GM integrity of mPFC predicts the degree of compromised SO-spindle dynamic coupling in older adults.

We implemented unique non-linear directional cross-frequency coupling (CFC) analyses, together with phase-dependent correlation measures, to capture complex neural dynamics underlying SO-spindle synchrony relationships (Helfrich and Knight, 2016). Based on theoretical accounts of oscillation-based timed memory transfer (Diekelmann and Born, 2010; Rasch and Born, 2013), we tested the hypothesis that the exact timing between SOs and spindles supports memory consolidation. Building on the prediction that SOs orchestrate sleep-dependent memory processing (Steriade, 2006), we implemented methods for assessing the temporal directionality of this SO-spindle interaction (Jiang et al., 2015) and examined whether this directionality predicted memory consolidation success in young and older adults. Finally, we tested whether regional GM atrophy within the mPFC, relative to other control regions, provided a structural correlate associated with the age-related degradation of SO-spindle coupling and associated memory decline in older adults.

RESULTS

Cognitively normal older ($n = 32$; age: 73.8 ± 5.3 ; mean \pm SD) and young ($n = 20$; 20.4 ± 2.0 years) participants performed a sleep-dependent episodic memory test (Mander et al., 2013, 2015) before and after a full night of sleep (Figure 1A; Tables S1–S3). During encoding, all participants were trained to 100% criterion before initial recognition testing (short delay; after ~ 10 min). After the short delay test, participants underwent polysomnography in the lab and were given an 8 hr sleep period starting at their habitual bedtime. They performed the second recognition test (long delay; after ~ 10 hr) the next morning. Then, structural MRI data to assess GM intensity were obtained. Memory retention was quantified as the difference between recognition performance at the long delay and performance at the short delay. Consistent with existing reports (Mander et al., 2013, 2017), overnight memory retention was impaired in older adults relative to young adults ($t_{46} = -3.85$, $p = 0.0004$, $d = 1.19$). Building on this finding, we next sought to determine differences in NREM oscillatory dynamics that may underlie these age-associated memory impairments.

Oscillatory Dynamics of Sleep in Old and Young Adults

We first assessed EEG power differences between older and young adults by means of cluster-based permutation tests across all frequencies and channels during NREM sleep (Figure 1B; with all figures displaying data from electrode Cz due to the spatial distribution of SO and spindle power, unless stated otherwise). Oscillatory power was significantly lower in older adults from 0.5 to 8.5 Hz ($p = 0.0020$, $d = 1.71$), as well as

between 10.5 and 15 Hz ($p = 0.0080$, $d = 1.28$), in all recorded channels (Figure 1B).

Next, we detected SO (0.16–1.25 Hz) and sleep spindle (12–16 Hz) events based on established algorithms (Möller et al., 2011; Staresina et al., 2015). Analysis of inter-spindle intervals indicated that sleep spindles exhibited non-Poisson-like behavior and were preferentially separated by 1.13–2.78 s during NREM sleep (Figure S1A), which is in accordance with the idea that <1 Hz SO controls sleep spindle timing and separates them by at least 1–3 cycles.

Detection of SO and sleep spindle events reliably tracked spectral sleep signatures over a full night of sleep (Figures 1C and 1D for representative old/young subjects; numbers of detected events are superimposed in white; see also Table S2). For every participant, we determined the SO phase during the peak of the detected sleep spindle events. Significant non-uniform circular distributions were identified in 29/32 old adults and in 20/20 young adults. Of note, differences in oscillatory power can distort CFC estimates. This issue was addressed by z-normalizing individual events in the time domain to alleviate amplitude differences prior to all subsequent analyses (Figure 2A; Table S4). Note that this normalization avoids spurious coupling that has been recently pointed out as a potential confound in cross-frequency analysis (Aru et al., 2015; Cole and Voytek, 2017; Gerber et al., 2016). To further address this concern, we also employed a validated stratification approach (Aru et al., 2015), confirming our main findings (Figures S1B and S1C).

Aging Affects Prefrontal SO-Spindle Coupling

Following normalization, SO trough-locked time-frequency spectrograms were first calculated separately for older and young adults and then compared using a cluster-based permutation approach. Multiple significant clusters were observed in the sleep spindle range (Figure 2B; $p = 0.0160$, $d = 1.73$). Interleaved patterning in the spindle range (white dashed box, Figure 2B) demonstrated that the timing of sleep spindles relative to the SOs was different between older and young adults. Specifically, spectrograms illustrated that sleep spindles peaked before, rather than in time with, the SO peak in older relative to young adults (Figure 2C, inset; Figure S2A).

Mean sleep spindle activity was nested just after the SO peak in young adults but was misaligned in older adults, occurring earlier in the rising flank of the SO (see Figures 2B and 2C). Significant non-uniform distributions were present for both older (Rayleigh $z = 23.24$, $p < 0.0001$) and young (Rayleigh $z = 18.55$, $p < 0.0001$) adults. However, the mean coupling direction differed significantly between groups (Figure 2D; older adults: $-46.3^\circ \pm 31.2^\circ$; young adults: $3.6^\circ \pm 15.5^\circ$; circular mean \pm SD; Watson-Williams test: $F_{1,50} = 41.34$; $p < 0.0001$; $\eta^2 = 0.44$). That is, spindles in young adults were maximal just after the SO peak, while sleep spindles in older adults were misaligned, prematurely peaking earlier on the rising phase in the SO cycle. This effect was not confounded by differences in spindle onset phase angles or differences in spindle duration (Figures S1D–S1F).

Next, we assessed differences in coupling strength between groups using two complimentary analyses: (1) an event-locked coupling approach that extracted the resultant vector length

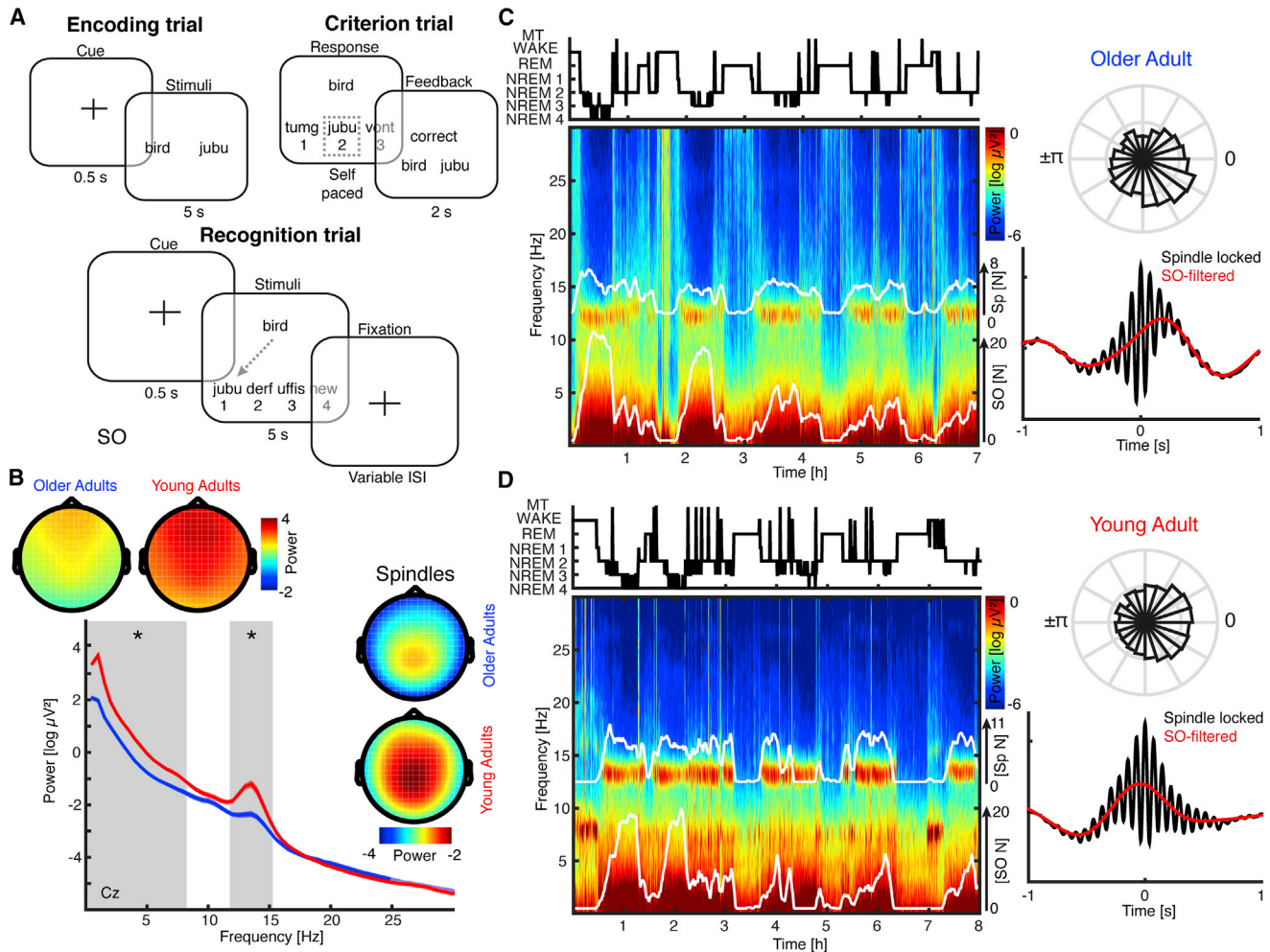


Figure 1. Memory Task and Oscillatory Signatures of Sleep

(A) Episodic word-pair task. Participants learned 120 word-nonsense word pairs. Nonsense words were 6–14 letters in length, derived from groups of common phonemes. During encoding trials (top left), word pairs were presented for 5 s. Participants completed the criterion training (top right) directly after encoding and received feedback after every trial. Recognition trials (bottom) were performed after a short delay (10 min, 45 trials) and again after a full night of sleep (10 hr, 135 trials).

(B) EEG power spectra during NREM sleep at electrode Cz for older (blue) and young (red) adults (mean \pm SEM). Gray shaded areas indicate significant differences in low and sleep spindle frequency ranges. Insets depict topographical distribution of SO (<1.5 Hz; upper topographies) and sleep spindle (12–16 Hz; lower topographies) power across the whole head. Note that older subjects exhibited significantly reduced oscillatory power across the whole head.

(C) Top left: hypnogram (MT, movement time) from one exemplary of older subject and full-night multi-taper spectrogram at Pz (bottom left) with superimposed number of detected SO and sleep spindle events (white solid lines; 5 min averages). Top right: normalized circular histogram of detected spindle events relative to the SO phase. Note the peak in the right lower quadrant. Bottom right: peak-locked sleep spindle average across all detected events in NREM sleep (black). Low-pass filtered events (red) highlight that the sleep spindles preferentially peaked prior to the SO “up-state.” See also Figure S1A.

(D) Exemplary young subject. Same conventions as in (C). Note that the sleep spindle amplitude is maximal after the SO peak.

per subject for all SO-spindle events at every electrode and (2) a data-driven approach based on the modulation index and screening of a wide range of phase-amplitude pairs.

For the first analysis, significant cluster difference in frontal topography was identified in older and young adults ($p = 0.0120$, $d = 0.76$), indicating that SO-spindle coupling was most impaired over fronto-central sensors (Figure 2E). The second, data-driven analysis confirmed that this fronto-central cluster effect was specific to the SO range between the 0.5–2 Hz and the 12–16 Hz range ($p = 0.0150$, $d = 0.92$), indi-

cating that stronger coupling in young adults was limited to the SO-spindle range (Figure 2F; Figure S2B). Both approaches were highly correlated ($\rho = 0.7645$, $p < 0.0001$), and effects were not simply driven by differences in the number of oscillatory events (Figures S1G and S1H).

Cortical Slow Oscillations Coordinate Spindle Activity

Having established differences in SO-spindle coupling between young and older adults, and building on our hypothesis and past theoretical models of SOs driving spindle coordination, we next

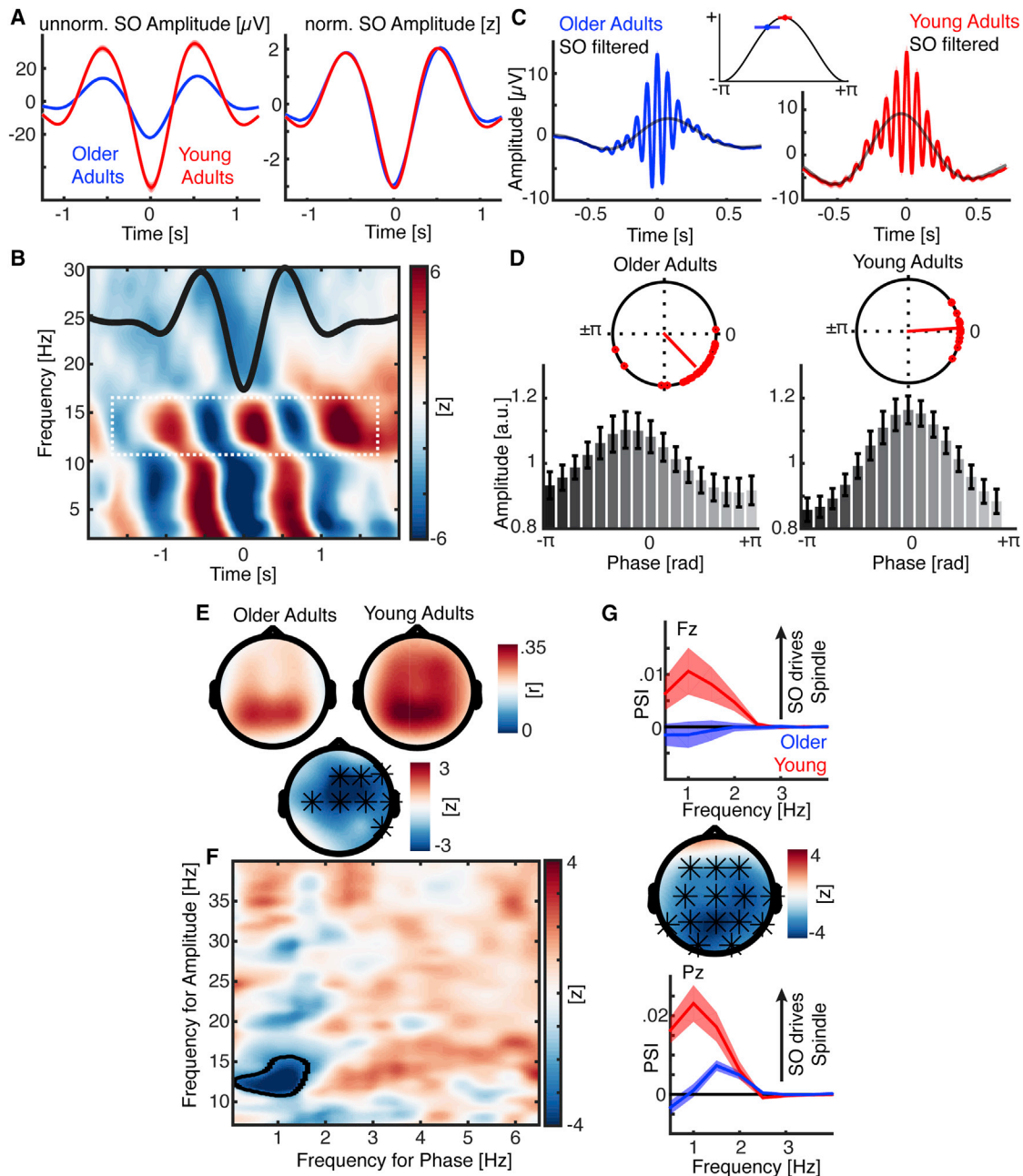


Figure 2. SO-Spindle Interactions in Old and Young Adults

(A) Left: trough-locked SO grand average for old (blue) and young (red) adults. Note the prominent differences in amplitude. Right: we normalized the SO amplitude for every subject prior to all other analyses to alleviate spurious effects, which could be the result of prominent power and signal-to-noise differences (mean \pm SEM).

(B) Statistical map of SO-locked power differences across time between older and young subjects. Note the interleaved patterning in the sleep spindle range (12–16 Hz; white dashed box). As reference, the mean SO is superimposed (black; rescaled). See also [Figure S2A](#).

(C) Left: peak-locked spindle grand averages for old adults with superimposed low-pass filtered signal (black). Right: peak-locked sleep spindle grand average for young adults. Top: averaging mean coupling phase and SD on schematic SO (cosine).

(D) Top: mean SO phase where sleep spindle power peaks. Red dots depict individual subjects. Note that sleep spindle power in older adults peaks prior to the SO positive peak (0°), while sleep spindle power in young subjects peaks around 0° . Bottom: grand-average normalized spindle amplitude binned relative to the SO phase (mean \pm SEM). Again, note the non-uniform distribution, which peaks around 0° for young adults, but earlier for older adults. See also [Figures S1D–S1H](#).

(E) Top: SO-spindle coupling strength (resultant vector length) topography for old (left) and young (right) adults. Bottom: a statistical difference map (center) indicates that the coupling strength was significantly reduced for fronto-central EEG sensors, while parieto-occipital estimates did not differ (* denotes cluster-corrected two-sided $p < 0.05$).

(legend continued on next page)

investigated directional influences between SOs and sleep spindles by means of the phase slope index (PSI).

A cluster-based permutation test revealed that the directional influence of SOs on sleep spindle activity was impaired in older relative to young adults over frontal and parieto-occipital regions (Figure 2G; $p = 0.0010$, $d = 0.81$). However, while parieto-occipital directional CFC was markedly reduced in older adults, it was still above zero (Figure S2C). This demonstrates that the parietal physiologic SO-spindle coupling was partially intact in older adults.

To examine directionality, we tested whether the PSI predicted how much time the sleep spindle deviated from the SO peak. A significant frontal cluster was identified over fronto-central sensors, indicating that larger PSI values predicted a smaller deviance—that is, a sleep spindle peak closer to the up-state in young relative to older adults ($p = 0.012$, mean $\rho = -0.3367$; older adults: 205.07 ± 18.68 ms; young adults: 60.24 ± 8.26 ms; mean \pm SD). This PSI analysis establishes two findings: (1) the SO phase predicts spindle timing over frontal sensors, rather than the converse, as postulated by theoretical models that SO triggers spindle events, and (2) the timing precision was misaligned, since directional influences were reduced in older relative to young adults.

SO-Spindle Coupling Predicts Overnight Memory Consolidation

Having characterized the oscillatory dynamics of SO-spindle coupling and identified impairments in these dynamics in older relative to young adults, we tested our hypothesis that these oscillatory dynamics predicted overnight memory retention success and associated age-related differences. Note that traditional linear correlation analyses were not applicable given that phase is a circular metric. Cluster-corrected circular-linear correlation analyses (see STAR Methods) were used to assess the non-linear relationship between optimal coupling phase and behavior.

A significant positive cluster was identified over frontal regions ($p = 0.0010$, mean $\rho = 0.4353$), peaking at electrode F3 ($\rho = 0.5699$; Figure 3A). To further delineate and visualize this non-linear relationship, we binned the average memory retention scores relative to the individual mean coupling direction (10 bins, overlap: ± 1 bin; gray shaded; Figure 3A). The resulting distribution followed an inverted u shape, demonstrating that the success of overnight memory consolidation was achieved when the spindle event occurred most proximal to the SO up-state peak. When spindles occurred further from that up-state peak, the predictive influence on overnight memory retention success declined. Note that this finding was not confounded by demographic or sleep architecture differences (Table S5).

No other significant EEG clusters were identified when SO-spindle coupling strength was correlated with the degree of overnight memory retention across all subjects (Figure 3B). To assure that these results were robust against differences in oscil-

lation power and peak frequency (Table S4), we corrected for sleep spindle peak and amplitude distribution confounds (Figure 3C; Figure S3) by detecting the individual sleep spindle peak frequency for every SO event. A significant positive cluster was observed ($p = 0.0040$, mean $\rho = 0.3790$), which peaked at electrode C4 (Figure 3D, $\rho = 0.4705$), indicating that the coupling phase robustly predicted overnight memory retention.

Importantly, this effect peaked in both older and young adults at neighboring electrodes (C4 in older adults: $\rho = 0.5725$; Cz in young adults: $\rho = 0.5678$). This result demonstrates that, even though older adults showed a reduction in SO-spindle coupling and lower overnight memory retention than young adults, the same predictive functional relationship between SO-spindle coupling and memory consolidation success was observed in both groups.

Performance for older and young adults was binned, allowing the expression of the quadratic fits to highlight the inverse u-shaped relationship indicated by the circular-linear correlations (Figure 3D). These findings confirmed that after correcting for power and peak frequency differences, the degree of overnight memory retention success was still predicted by the timing of the coupled relationship between the SO and the spindle (Figure 3D). Therefore, memory consolidation success was most accurately predicted by sleep spindle amplitude peaking just after the SO up-state peak.

Age-Related Gray Matter Atrophy Predicts Coupling Deficits

Collectively, the above analyses (1) establish that the oscillatory dynamics of SO-spindle coupling demonstrate impairments in these dynamics in older relative to young adults and (2) identify that the spatiotemporal precision of SO-spindle coupling predicts the degree of overnight memory retention success and, when impaired in older adults, predicts greater overnight forgetting.

Finally, we sought to determine a potential underlying pathological mechanism accounting for why older adults suffer these impairments. We focused *a priori* on mPFC GM, based on the prominent role of the mPFC in SO oscillatory generation (Murphy et al., 2009; Saletin et al., 2013). Specifically, we tested the hypothesis that mPFC GM atrophy predicts the degree of compromised SO-spindle dynamic coupling.

To rule out age-related confounds, we corrected all structural metrics by the total intracranial volume, which were correlated ($\rho = -0.2919$, $p = 0.0358$). We then utilized cluster-based permutation correlation analyses to assess whether the GM volume in any region of interest (ROI) predicted directional SO-spindle coupling as measured by the PSI. Consistent with the hypothesis, GM volume in mPFC positively correlated with directional coupling (Figure 4A; $p = 0.0080$, mean $\rho = 0.3321$), indicating that as GM volume in mPFC decreases, directional phase

(F) Statistical map of a data-driven comodulogram. The black-circled area highlights the significant difference between older and young adults, which was confined to the SO-spindle range. See also Figure S2B.

(G) Cross-frequency directionality analyses. Values above zero indicate that SOs drive sleep spindle activity. Top: we found that frontal SOs drive sleep spindle activity in young, but not older, adults (electrode Fz; mean \pm SEM), while parieto-occipital SO predicts sleep spindle activity in both older and young adults (bottom; Pz; Figure S2C). However, this effect is pronounced for young adults. The topography (middle) depicts the spatial extent where directional SO-spindle influences are reduced in older relative to young adults. Note that this effect was independent of the chosen window length (Figure S2D).

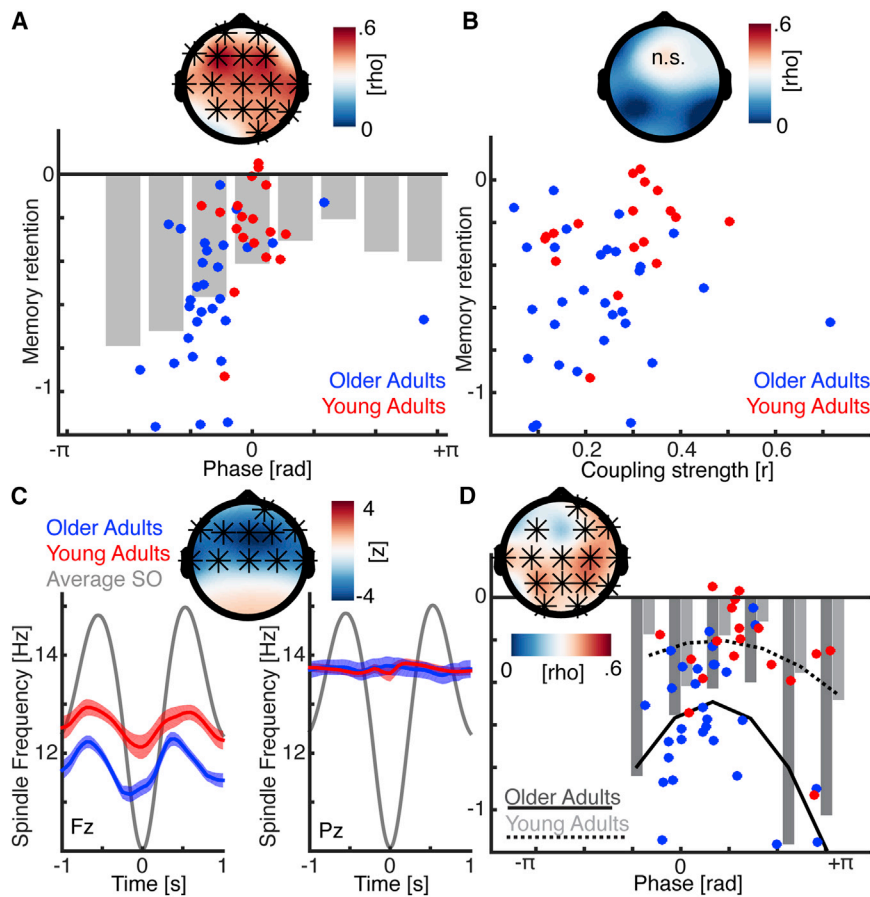


Figure 3. Timing of SO-Spindle Interactions Predicts Memory Retention

(A) Top: cluster-corrected circular-linear correlation analysis between the individual mean SO-spindle coupling phase and overnight memory retention after correction for power differences (* indicates significant sensors). The strongest effect was observed at electrode F3. Bottom: blue dots indicate older adults; red dots young adults. We binned the mean behavioral performance relative to the coupling phase in ten overlapping bins to highlight the u-shaped, non-linear relationship.

(B) No significant correlation was observed between coupling strength (resultant vector length) and memory retention (same conventions as in A). (C) Sleep spindle frequency relative to SO cycle at a frontal (left) and parieto-occipital (Pz; right) electrode (mean \pm SEM). Frontal sleep spindles are slower than posterior sleep spindles. Their frequency only varies as a function of the SO phase over frontal regions, where it is significantly lower for older adults (top).

(D) Cluster-corrected circular-linear correlations after correcting for differences in power distributions and sleep spindle frequencies (see also Figure S3; same conventions as in A). Importantly, memory retention was coupling phase dependent in older and young adults. Overall, the best performance was observed when the sleep spindles peak just after the SO peak. Blue dots depict older adults. Dark gray bars indicate mean binned memory performance; black solid line depicts a quadratic fit to approximate the non-linear, u-shaped relationship. Conversely, red dots, light gray bars, and the dashed black line reflect young adults.

coupling between SOs and sleep spindles is weakened. Note that the results were comparable when we corrected for total brain volume ($\rho = 0.29$, $p = 0.0343$). In addition, we partialled out age from the cluster-based correlation test (see STAR Methods) and again obtained a significant frontal cluster ($p = 0.0490$; mean $\rho = 0.25$).

While our results confirmed the key role of SOs in the coupling dynamics and associated memory consolidation benefit, sleep spindles, which are grouped by the SOs, are anatomically recognized to be thalamo-cortical-mediated events (Steriade et al., 1987; though spindles have also been measured in the hippocampus; De Gennaro and Ferrara, 2003; Staresina et al., 2015). Given these findings, we performed additional post hoc analyses to examine whether GM volume in these spindle-associated regions also predicted impairments in SO-spindle coupling.

GM volume was extracted for all ROIs where sleep-related oscillations are thought to emerge: hippocampus and the thalamus, in addition to the neighboring lateral orbitofrontal cortex (OFC) or dorsolateral PFC (DLPFC) and several control ROIs (occipital, precuneus, posterior cingulate cortex, and posterior parietal cortex), but no significant effects were observed for these other eight ROIs (Figure 4B). These results confirmed the key role of mPFC in altered SO-spindle coupling—an anatomical-physiological relationship that was not observed for other likely candidate regions.

DISCUSSION

Together, our results provide the first demonstration that (1) the precisely coordinated timing between the cortical NREM SO up-state and the sleep spindle predicts successful hippocampus-dependent memory consolidation; (2) temporal disruption of this coordinated NREM oscillation coupling in older relative to young adults predicts impaired hippocampus-dependent overnight memory consolidation; and (3) one pathological mechanism associated with impairment in spatiotemporal coupling of the cortical SOs with sleep spindles in older adults is the severity of mPFC GM atrophy.

The Oscillatory Hierarchy of Sleep-Dependent Memory Consolidation

A long-standing proposal in models of sleep-dependent, hippocampus-dependent memory consolidation involves the timed interactive coupling between SOs and sleep spindles (Rasch and Born, 2013). Indirect evidence to date has involved demonstrating that individual properties of SOs and sleep spindles are linked to successful overnight memory retention (Niknazar et al., 2015; Mander et al., 2013; Gais et al., 2002; Mander et al., 2014; Mölle et al., 2002). Seminal intracranial EEG studies have further highlighted the hierarchical coupling of cortical SOs, cortico-thalamic sleep spindles, and hippocampal

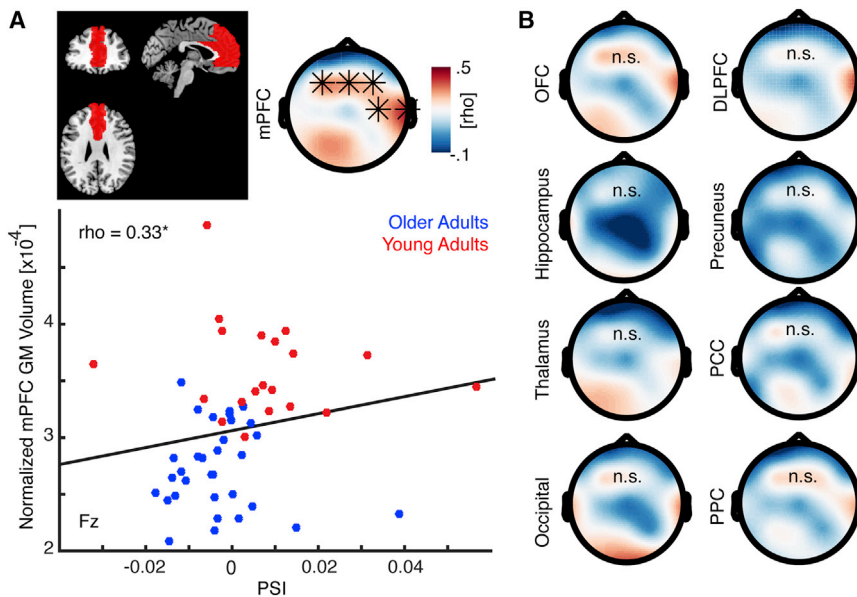


Figure 4. Directional SO-Spindle Coupling Depends on Prefrontal Gray Matter Volume

(A) Top right: definition of the mPFC ROI on coronal, sagittal, and axial slices. Top left: topographic map of cluster-corrected correlation analysis between gray matter (GM) volume and the directional CFC (PSI), which revealed that directional influences were stronger when subjects had more GM volume. Bottom: scatterplot of significant correlation at electrode Fz. Hence, age-related GM atrophy contributes to a breakdown of SO-mediated spindle coupling. Note that GM volume was corrected for age-related total intracranial volume.

(B) This significant relationship was limited to mPFC and was not observed in other select regions, including the hippocampus, thalamus, adjacent regions, such as the OFC and DLPFC, or in any of additional control regions (occipital, precuneus, posterior cingulate, and posterior parietal).

ripples (Clemens et al., 2007; Mak-McCully et al., 2017; Staresina et al., 2015). However, no assessment of memory was performed in these studies, leaving the functional relevance of these coupled NREM oscillation relationships unclear. Moreover, no direct assessment of the directionality of the coupling of these events has been reported.

Here, we address these issues using directional CFC analyses (Helfrich and Knight, 2016) and determine how SOs modulate sleep spindle timing, amplitude, and peak frequency. Our results reveal a unique spatiotemporal profile of the coupling relationship between SOs and sleep spindles in young adults, such that sleep spindle amplitude peaked around the cortical up-state. Moreover, this precise temporal relationship was especially pronounced over centro-parietal regions—of topographical relevance as it may be considered the anatomical convergence zone between the known frontal dominance of the SOs (Murphy et al., 2009) and the parietal dominance of broad-range (11–16 Hz) spindles (De Gennaro and Ferrara, 2003; Riedner et al., 2011).

A second key finding revealed by the current study is that the normally precise spatiotemporal coordination of the SO-spindle-coupled event is impaired in older adults. Unlike young adults, in which spindle events expressed a strong coincidence with the cortical SO up-state, spindle oscillations in older adults arrived significantly further away from the depolarizing upswing of the SO cycle, occurring prior to it rather than just after the depolarization envelop. In addition, this phase coupling was more dispersed over SOs in older adults. These findings provide evidence that the aging brain loses the neurophysiological ability to coordinate the two dominant oscillations of NREM sleep, in stark contrast to the precise spatiotemporal coupling expressed in young adults. However, these data alone do not necessarily establish that this dynamic coupling profile is of functional benefit in young adults and whether coupling impairments in older adults is detrimental for older adults. We address this issue next.

SO-Spindle Coupling and Overnight Memory Consolidation

System consolidation theory suggests that new memories are transiently more dependent on the hippocampus and then gradually transform to become more prefrontal dependent (Frankland and Bontempi, 2005; Kitamura et al., 2017). Endogenous NREM oscillatory activity is thought to provide the key functional substrate of timed information transfer between cortical regions (Buzsáki and Draguhn, 2004). In particular, neocortical SOs are thought to orchestrate thalamo-cortical sleep spindle and hippocampal ripple activity during NREM sleep to facilitate the information transfer between neocortical and hippocampal circuits (Buzsáki, 1998; Isomura et al., 2006; Sirota et al., 2003). This nesting of multiple frequency bands constitutes an oscillatory hierarchy, providing the precise intrinsically generated timing to route information from the hippocampus to neocortical areas at times of high excitability, which in turn facilitate long-term storage (Born and Wilhelm, 2012; Diekelmann and Born, 2010).

Several studies have inferred a role of the phase of the SO in determining the success of memory consolidation using indirect measures (Batterink et al., 2016; Papalambros et al., 2017). In addition, brain stimulation studies have established that entrainment of SOs can have reciprocal effects on sleep spindles and vice versa (Lustenberger et al., 2016; Marshall et al., 2006). Most recently, it has been suggested that shifts in the exact SO-spindle timing could give rise to the behavioral benefits of electrical stimulation observed in rodents, which may also be beneficial in cognitively impaired older individuals (Ladenbauer et al., 2017; Latchoumane et al., 2017; Niknazar et al., 2015). Our results provide the first direct evidence that the exact timing of SOs and sleep spindles in the healthy, human brain predicts the success of overnight hippocampus-dependent memory retention (Diekelmann and Born, 2010; Mander et al., 2017).

A further discovery of the current study is the demonstration that the precise temporal interplay of SOs and sleep spindles is disrupted in older adults, wherein sleep spindles were

misaligned (often occurring too early in the SO cycle) relative to the precise timing in young adults. The process of human brain aging appears to weaken the otherwise robust NREM oscillatory hierarchy, reducing the optimal SO-spindle phase timing, and, in doing so, predicts impaired memory consolidation. Two points are of relevance in this regard. First, the finding that the memory-SO-spindle coupling relationship was significant in older adults, but at an earlier phase, demonstrates that both SOs and sleep spindles were still expressed in older adults. However, the mechanism that couples them in time is impaired, with spindles systematically arriving too early within the SO cycle. Second, it establishes that this impaired SO-spindle temporal coupling diminished the magnitude of overnight memory consolidation benefit.

Neurophysiological Correlates of Age-Related Memory Decline

A multitude of studies demonstrated that aging affects sleep architecture and memory (Mander et al., 2017). However, no neurophysiological mechanism has been identified that functionally links age-related changes in sleep physiology to impaired memory retention, beyond quantitative reductions in the amount of oscillatory activity. Here, we provide evidence that addresses this mechanistic gap in understanding, demonstrating that the loss of temporal SO-spindle coupling over specific topographical regions explains the degree of failed memory consolidation.

Interestingly, when only focusing on the basic phase measure, sleep spindles lock as precisely to the rising flank of the SOs in older adults as they do young adults, as we show in Figures 2C and 2D. However, our directional phase analyses revealed the existence of a clear age-related deficit. Specifically, inspection of SO-spindle interactions, shown in Figure 2G, demonstrated that the directional influence of SOs on sleep spindle timing was diminished in older adults relative to young adults, resulting in a misaligned arrival of the spindle relative to the SO. Moreover, we found that this age-related impairment was not equivalent across all brain regions but was expressed most significantly over prefrontal cortex sensors and less strongly over parieto-occipital regions (Figure 2G; Figure S2C). These results further establish that, in later adult life, the human adult brain experiences a decline in the ability to precisely coordinate SOs with cortico-thalamic sleep spindles. Specifically, spindles occur more often at unfavorable SO phases in older adults, arriving too early to confer optimal hippocampus-dependent memory consolidation benefits.

One testable hypothesis in animal models emerging from our findings is that the impaired coordination of temporal SO-spindle coupling over prefrontal cortex does not trigger hippocampal ripples as effectively and that the magnitude of that failure should predict the consequential degree of impaired rather than successful sleep-dependent memory consolidation (Rosanova and Ulrich, 2005).

Prefrontal Atrophy, SO-Spindle Coupling, and Aging

Beyond impairments in memory-relevant SO-spindle coupling in older relative to young adults, we further established at least one pathological alteration contributing to the severity of this age-related coupling dysfunction—GM atrophy within the mPFC.

GM volume of the mPFC predicts inter-individual differences in the quality of SOs in both young (Saletin et al., 2013) and older (Mander et al., 2013) adults. Moreover, high-density EEG evidence has defined a role for the mPFC in the generation of slow waves (Murphy et al., 2009).

Our findings advance this anatomical-neurophysiological connection. We show that the decrease in structural integrity of the mPFC accounts for the qualitative degree of impaired temporal phase coupling between the SOs and sleep spindles. Thus, mPFC atrophy, in addition to reducing SO incidence and intensity (Mander et al., 2013; Saletin et al., 2013), contributes to misalignment of the timing of sleep spindles relative to the SO phase. This effect is greatest over frontal EEG derivations, indicating that the mPFC may play a particularly important role in the regulation of the coordinated timing of NREM sleep oscillations.

The results reveal that the structural integrity of mPFC is one factor determining the capacity of the human brain to precisely and optimally coordinate the timed arrival of sleep spindles with the SOs and, in doing so, dictate the success or failure of hippocampus-dependent memory consolidation. Intracranial studies taking advantage of invasive recordings from multiple ROIs in concert, such as mPFC, the hippocampus, and thalamus (Clemens et al., 2007; Mak-McCully et al., 2017; Nir et al., 2011; Staesina et al., 2015), will help to clarify the directional influences of cortical-subcortical interaction not possible with scalp EEG recordings. Such recordings occurring combined with sleep-dependent memory tasks would further our current understanding of the coordinated interactions between the mPFC, thalamus, and hippocampus that occurs during NREM sleep oscillations as well as their necessity and sufficiency in supporting long-term memory retention.

Conclusions

Our findings reveal a fundamental neurophysiologic mechanism involving the spatiotemporal coupling between the SO and the sleep spindle and demonstrate that this temporal synchrony is functionally and behaviorally relevant for the success of overnight memory consolidation. We further show that this same neurophysiological oscillatory dynamic is impaired in older relative to young adults, leading to imprecise sleep spindle expression in relationship with the depolarizing up-state of the SO. Moreover, our findings reveal that age-related prefrontal GM atrophy represents one neuropathological substrate explaining the attenuation of this oscillatory control mechanism, which thus impairs hippocampus-dependent memory consolidation.

Our results are of potential clinical relevance in two ways. First, they document the presence of an under-appreciated pathway—impaired temporal precision of sleep oscillation coupling—that contributes to memory decline in later life. Second, they help define sleep oscillatory synchrony as a novel therapeutic target for modulation of hippocampus-dependent memory consolidation in older adults and potentially in those with mild cognitive impairment (Ladenbauer et al., 2017) and Alzheimer's disease (Mander et al., 2017). This may be achieved using non-invasive entrainment by means of acoustic, electric, or magnetic brain stimulation (Helfrich et al., 2014; Papalambros et al., 2017), aiming to restore the temporally precise SO-spindle coordination

(Marshall et al., 2006) closer to that of young adults, helping reduce the impact of cognitive decline in aging.

STAR★METHODS

Detailed methods are provided in the online version of this paper and include the following:

- KEY RESOURCES TABLE
- CONTACT FOR REAGENT AND RESOURCE SHARING
- EXPERIMENTAL MODEL AND SUBJECT DETAILS
 - Participants
- METHOD DETAILS
 - Experimental Design and Procedure
 - Behavioral Task
 - Sleep Monitoring and EEG Data Acquisition
 - MRI Data Acquisition
- QUANTIFICATION AND STATISTICAL ANALYSIS
 - Behavioral Data Analysis
 - EEG Data
 - Structural MRI Data Analysis
 - Statistical Analysis
- DATA AND SOFTWARE AVAILABILITY

SUPPLEMENTAL INFORMATION

Supplemental Information includes three figures and five tables and can be found with this article online at <https://doi.org/10.1016/j.neuron.2017.11.020>.

AUTHOR CONTRIBUTIONS

Conceptualization, R.F.H., B.A.M., W.J.J., R.T.K., and M.P.W.; Methodology, R.F.H.; Software, R.F.H. and B.A.M.; Validation, R.F.H. and B.A.M.; Formal Analysis, R.F.H. and B.A.M.; Investigation, B.A.M.; Resources, W.J.J., R.T.K., and M.P.W.; Data Curation, R.F.H., B.A.M., and M.P.W.; Writing – Original Draft, R.F.H.; Writing – Review & Editing, R.F.H., B.A.M., R.T.K., and M.P.W.; Visualization, R.F.H.; Supervision, R.T.K. and M.P.W.; Project Administration, B.A.M. and M.P.W.; Funding Acquisition, W.J.J., R.T.K., and M.P.W.

ACKNOWLEDGMENTS

This work was supported by the Alexander von Humboldt Foundation (Feodor Lynen Program; R.F.H.), an intramural fellowship from the Dept. of Psychology, University of Oslo (R.F.H.), and R37NS21135 (R.T.K.), R01AG034570 (W.J.J.), R01AG031164 (M.P.W.), R01AG054019 (M.P.W.), RF1AG054019 (M.P.W.), R01MH093537 (M.P.W.), and F32-AG039170 (B.A.M.), all from the National Institutes of Health. We thank Joe Winer, David Baquirin, Maggie Belshe, Meghna Bhatler, Michelle Binod, Sam Bowditch, Catherine Dang, Jay Gupta, Amynta Hayenga, Danny Holzman, April Horn, Emily Hur, Jonathan Jeng, Samika Kumar, Candace Markeley, Elizabeth Mormino, Molly Nicholas, Sina Rashidi, Matthew Shonman, Lily Zhang, and Alyssa Zhu for their assistance and Anthony Mander for his aid in task design.

Received: August 28, 2017

Revised: October 23, 2017

Accepted: November 14, 2017

Published: December 14, 2017

REFERENCES

Aru, J., Aru, J., Priesemann, V., Wibral, M., Lana, L., Pipa, G., Singer, W., and Vicente, R. (2015). Untangling cross-frequency coupling in neuroscience. *Curr. Opin. Neurobiol.* 31, 51–61.

Ashburner, J., and Friston, K.J. (2000). Voxel-based morphometry—the methods. *Neuroimage* 11, 805–821.

Batterink, L.J., Creery, J.D., and Paller, K.A. (2016). Phase of spontaneous slow oscillations during sleep influences memory-related processing of auditory cues. *J. Neurosci.* 36, 1401–1409.

Berens, P. (2009). CircStat: a MATLAB toolbox for circular statistics. *J. Stat. Softw.* 31, 21.

Born, J., and Wilhelm, I. (2012). System consolidation of memory during sleep. *Psychol. Res.* 76, 192–203.

Brett, M., Anton, J.-L., Valabregue, R., and Poline, J.-B. (2002). Region of interest analysis using the MarsBar toolbox for SPM 99. *Neuroimage* 16, S497.

Buzsáki, G. (1998). Memory consolidation during sleep: a neurophysiological perspective. *J. Sleep Res.* 7 (Suppl 1), 17–23.

Buzsáki, G., and Draguhn, A. (2004). Neuronal oscillations in cortical networks. *Science* 304, 1926–1929.

Canolty, R.T., Edwards, E., Dalal, S.S., Soltani, M., Nagarajan, S.S., Kirsch, H.E., Berger, M.S., Barbaro, N.M., and Knight, R.T. (2006). High gamma power is phase-locked to theta oscillations in human neocortex. *Science* 313, 1626–1628.

Clemens, Z., Mölle, M., Eross, L., Barsi, P., Halász, P., and Born, J. (2007). Temporal coupling of parahippocampal ripples, sleep spindles and slow oscillations in humans. *Brain* 130, 2868–2878.

Cole, S.R., and Voytek, B. (2017). Brain oscillations and the importance of waveform shape. *Trends Cogn. Sci.* 21, 137–149.

De Gennaro, L., and Ferrara, M. (2003). Sleep spindles: an overview. *Sleep Med. Rev.* 7, 423–440.

Delorme, A., and Makeig, S. (2004). EEGLAB: an open source toolbox for analysis of single-trial EEG dynamics including independent component analysis. *J. Neurosci. Methods* 134, 9–21.

Diekelmann, S., and Born, J. (2010). The memory function of sleep. *Nat. Rev. Neurosci.* 11, 114–126.

Dvorak, D., and Fenton, A.A. (2014). Toward a proper estimation of phase-amplitude coupling in neural oscillations. *J. Neurosci. Methods* 225, 42–56.

Flinker, A., Korzeniewska, A., Shestyuk, A.Y., Franaszczuk, P.J., Dronkers, N.F., Knight, R.T., and Crone, N.E. (2015). Redefining the role of Broca's area in speech. *Proc. Natl. Acad. Sci. USA* 112, 2871–2875.

Frankland, P.W., and Bontempi, B. (2005). The organization of recent and remote memories. *Nat. Rev. Neurosci.* 6, 119–130.

Gais, S., Mölle, M., Helms, K., and Born, J. (2002). Learning-dependent increases in sleep spindle density. *J. Neurosci.* 22, 6830–6834.

Gerber, E.M., Sadeh, B., Ward, A., Knight, R.T., and Deouell, L.Y. (2016). Non-sinusoidal activity can produce cross-frequency coupling in cortical signals in the absence of functional interaction between neural sources. *PLoS ONE* 11, e0167351.

Helfrich, R.F., and Knight, R.T. (2016). Oscillatory dynamics of prefrontal cognitive control. *Trends Cogn. Sci.* 20, 916–930.

Helfrich, R.F., Schneider, T.R., Rach, S., Trautmann-Lengsfeld, S.A., Engel, A.K., and Herrmann, C.S. (2014). Entrainment of brain oscillations by transcranial alternating current stimulation. *Curr. Biol.* 24, 333–339.

Helfrich, R.F., Huang, M., Wilson, G., and Knight, R.T. (2017). Prefrontal cortex modulates posterior alpha oscillations during top-down guided visual perception. *Proc. Natl. Acad. Sci. USA* 114, 9457–9462.

Isomura, Y., Sirota, A., Ozen, S., Montgomery, S., Mizuseki, K., Henze, D.A., and Buzsáki, G. (2006). Integration and segregation of activity in entorhinal-hippocampal subregions by neocortical slow oscillations. *Neuron* 52, 871–882.

Jiang, H., Bahramisharif, A., van Gerven, M.A.J., and Jensen, O. (2015). Measuring directionality between neuronal oscillations of different frequencies. *Neuroimage* 118, 359–367.

Kitamura, T., Ogawa, S.K., Roy, D.S., Okuyama, T., Morrissey, M.D., Smith, L.M., Redondo, R.L., and Tonegawa, S. (2017). Engrams and circuits crucial for systems consolidation of a memory. *Science* 356, 73–78.

- Ladenbauer, J., Ladenbauer, J., Kützow, N., de Boor, R., Avramova, E., Grittner, U., and Flöel, A. (2017). Promoting sleep oscillations and their functional coupling by transcranial stimulation enhances memory consolidation in mild cognitive impairment. *J. Neurosci.* *37*, 7111–7124.
- Latchoumane, C.V., Ngo, H.-V.V., Born, J., and Shin, H.-S. (2017). Thalamic spindles promote memory formation during sleep through triple phase-locking of cortical, thalamic, and hippocampal rhythms. *Neuron* *95*, 424–435.e6.
- Lustenberger, C., Boyle, M.R., Alagapan, S., Mellin, J.M., Vaughn, B.V., and Fröhlich, F. (2016). Feedback-controlled transcranial alternating current stimulation reveals a functional role of sleep spindles in motor memory consolidation. *Curr. Biol.* *26*, 2127–2136.
- Mak, H.K.-F., Zhang, Z., Yau, K.K.-W., Zhang, L., Chan, Q., and Chu, L.-W. (2011). Efficacy of voxel-based morphometry with DARTEL and standard registration as imaging biomarkers in Alzheimer's disease patients and cognitively normal older adults at 3.0 Tesla MR imaging. *J. Alzheimers Dis.* *23*, 655–664.
- Mak-McCully, R.A., Rolland, M., Sargsyan, A., Gonzalez, C., Magnin, M., Chauvel, P., Rey, M., Bastuji, H., and Halgren, E. (2017). Coordination of cortical and thalamic activity during non-REM sleep in humans. *Nat. Commun.* *8*, 15499.
- Maldjian, J.A., Laurienti, P.J., Kraft, R.A., and Burdette, J.H. (2003). An automated method for neuroanatomic and cytoarchitectonic atlas-based interrogation of fMRI data sets. *Neuroimage* *19*, 1233–1239.
- Mander, B.A., Rao, V., Lu, B., Saletin, J.M., Lindquist, J.R., Ancoli-Israel, S., Jagust, W., and Walker, M.P. (2013). Prefrontal atrophy, disrupted NREM slow waves and impaired hippocampal-dependent memory in aging. *Nat. Neurosci.* *16*, 357–364.
- Mander, B.A., Rao, V., Lu, B., Saletin, J.M., Ancoli-Israel, S., Jagust, W.J., and Walker, M.P. (2014). Impaired prefrontal sleep spindle regulation of hippocampal-dependent learning in older adults. *Cereb. Cortex* *24*, 3301–3309.
- Mander, B.A., Marks, S.M., Vogel, J.W., Rao, V., Lu, B., Saletin, J.M., Ancoli-Israel, S., Jagust, W.J., and Walker, M.P. (2015). β -amyloid disrupts human NREM slow waves and related hippocampus-dependent memory consolidation. *Nat. Neurosci.* *18*, 1051–1057.
- Mander, B.A., Winer, J.R., and Walker, M.P. (2017). Sleep and human aging. *Neuron* *94*, 19–36.
- Maris, E., and Oostenveld, R. (2007). Nonparametric statistical testing of EEG- and MEG-data. *J. Neurosci. Methods* *164*, 177–190.
- Marshall, L., Helgadóttir, H., Mölle, M., and Born, J. (2006). Boosting slow oscillations during sleep potentiates memory. *Nature* *444*, 610–613.
- Mitra, P.P., and Pesaran, B. (1999). Analysis of dynamic brain imaging data. *Biophys. J.* *76*, 691–708.
- Mölle, M., Marshall, L., Gais, S., and Born, J. (2002). Grouping of spindle activity during slow oscillations in human non-rapid eye movement sleep. *J. Neurosci.* *22*, 10941–10947.
- Mölle, M., Bergmann, T.O., Marshall, L., and Born, J. (2011). Fast and slow spindles during the sleep slow oscillation: disparate coalescence and engagement in memory processing. *Sleep* *34*, 1411–1421.
- Murphy, M., Riedner, B.A., Huber, R., Massimini, M., Ferrarelli, F., and Tononi, G. (2009). Source modeling sleep slow waves. *Proc. Natl. Acad. Sci. USA* *106*, 1608–1613.
- Niknazar, M., Krishnan, G.P., Bazhenov, M., and Mednick, S.C. (2015). Coupling of thalamocortical sleep oscillations are important for memory consolidation in humans. *PLoS ONE* *10*, e0144720.
- Nir, Y., Staba, R.J., Andrillon, T., Vyazovskiy, V.V., Cirelli, C., Fried, I., and Tononi, G. (2011). Regional slow waves and spindles in human sleep. *Neuron* *70*, 153–169.
- Oostenveld, R., Fries, P., Maris, E., and Schoffelen, J.-M. (2011). FieldTrip: open source software for advanced analysis of MEG, EEG, and invasive electrophysiological data. *Comput. Intell. Neurosci.* *2011*, 156869.
- Papalambros, N.A., Santostasi, G., Malkani, R.G., Braun, R., Weintraub, S., Paller, K.A., and Zee, P.C. (2017). Acoustic enhancement of sleep slow oscillations and concomitant memory improvement in older adults. *Front. Hum. Neurosci.* *11*, 109.
- Penny, W.D., Friston, K.J., Ashburner, J.T., Kiebel, S.J., and Nichols, T.E. (2011). *Statistical Parametric Mapping: The Analysis of Functional Brain Images* (Academic Press).
- Prerau, M.J., Brown, R.E., Bianchi, M.T., Ellenbogen, J.M., and Purdon, P.L. (2017). Sleep neurophysiological dynamics through the lens of multitaper spectral analysis. *Physiology* (Bethesda) *32*, 60–92.
- Rajapakse, J.C., Giedd, J.N., and Rapoport, J.L. (1997). Statistical approach to segmentation of single-channel cerebral MR images. *IEEE Trans. Med. Imaging* *16*, 176–186.
- Rasch, B., and Born, J. (2013). About sleep's role in memory. *Physiol. Rev.* *93*, 681–766.
- Rechtschaffen, A., and Kales, A. (1968). *A Manual of Standardized Terminology, Techniques, and Scoring Systems for Sleep Stages of Human Subjects* (Public Health Service, US Government Printing Office).
- Riedner, B.A., Hulse, B.K., Murphy, M.J., Ferrarelli, F., and Tononi, G. (2011). Temporal dynamics of cortical sources underlying spontaneous and peripherally evoked slow waves. *Prog. Brain Res.* *193*, 201–218.
- Rosanova, M., and Ulrich, D. (2005). Pattern-specific associative long-term potentiation induced by a sleep spindle-related spike train. *J. Neurosci.* *25*, 9398–9405.
- Saletin, J.M., van der Helm, E., and Walker, M.P. (2013). Structural brain correlates of human sleep oscillations. *Neuroimage* *83*, 658–668.
- Sirota, A., Csicsvari, J., Buhl, D., and Buzsáki, G. (2003). Communication between neocortex and hippocampus during sleep in rodents. *Proc. Natl. Acad. Sci. USA* *100*, 2065–2069.
- Staresina, B.P., Bergmann, T.O., Bonfond, M., van der Meij, R., Jensen, O., Deuker, L., Elger, C.E., Axmacher, N., and Fell, J. (2015). Hierarchical nesting of slow oscillations, spindles and ripples in the human hippocampus during sleep. *Nat. Neurosci.* *18*, 1679–1686.
- Steriade, M. (2006). Grouping of brain rhythms in corticothalamic systems. *Neuroscience* *137*, 1087–1106.
- Steriade, M., Domich, L., Oakson, G., and Deschênes, M. (1987). The deafferented reticular thalamic nucleus generates spindle rhythmicity. *J. Neurophysiol.* *57*, 260–273.
- Tzourio-Mazoyer, N., Landeau, B., Papathanassiou, D., Crivello, F., Etard, O., Delcroix, N., Mazoyer, B., and Joliot, M. (2002). Automated anatomical labeling of activations in SPM using a macroscopic anatomical parcellation of the MNI MRI single-subject brain. *Neuroimage* *15*, 273–289.
- Walker, M.P., and Stickgold, R. (2006). Sleep, memory, and plasticity. *Annu. Rev. Psychol.* *57*, 139–166.
- Wen, H., and Liu, Z. (2016). Separating fractal and oscillatory components in the power spectrum of neurophysiological signal. *Brain Topogr.* *29*, 13–26.

STAR★METHODS

KEY RESOURCES TABLE

REAGENT or RESOURCE	SOURCE	IDENTIFIER
Software and Algorithms		
MATLAB 2015a	MathWorks	RRID: SCR_001622
EEGLAB 13_4_4b	Delorme and Makeig, 2004	https://sccn.ucsd.edu/eeglab/index.php
FieldTrip 20161016	Oostenveld et al., 2011	http://www.fieldtriptoolbox.org/
CircStat 2012	Berens, 2009	https://philippberens.wordpress.com/code/circstats/
IRASA	Wen and Liu, 2016	https://purr.purdue.edu/publications/1987/1
SPM8	Penny et al., 2011	http://www.fil.ion.ucl.ac.uk/spm/
VBM8	Ashburner and Friston, 2000	http://dbm.neuro.uni-jena.de/vbm.html
DARTEL	Mak et al., 2011	Included in SPM
Anatomical Automatic Labeling	Tzourio-Mazoyer et al., 2002	Included in SPM
Wake Forest University PickAtlas	Maldjian et al., 2003	http://fmri.wfubmc.edu/software/pickatlas
Marsbar	Brett et al., 2002	http://marsbar.sourceforge.net/

CONTACT FOR REAGENT AND RESOURCE SHARING

Further information and requests for resources and reagents should be directed to and will be fulfilled by the lead contact, Randolph Helfrich (rhelfrich@berkeley.edu).

EXPERIMENTAL MODEL AND SUBJECT DETAILS

Participants

32 healthy older (mean age: 73.7 ± 5.3 ; mean \pm SD) and 20 younger adults (20.4 ± 2.0 years) participated in the study (see [Table S1](#) for demographic details). All participants provided written informed consent according to the local ethics committee (Berkeley Committee for Protection of Human Subjects Protocol Number 2010-01-595) and the Declaration of Helsinki. Data from a subset of participants has been reported previously ([Mander et al., 2013, 2014, 2015](#)).

METHOD DETAILS

Experimental Design and Procedure

All participants were trained on the episodic word-pair task in the evening and performed a short recognition test after 10 min. Then, participants were offered an 8 hr sleep opportunity, starting at their habitual bedtime. Polysomnography was collected continuously. Participants performed a long version of the recognition test approximately 2 hr after awakening. Subsequently, we obtained structural MRI scans from all participants. Two older adults did not complete behavioral testing, and two young adults failed to achieve criterion at encoding. Thus, these four subjects were excluded from behavioral analyses, but were included in all electrophysiological and imaging analyses.

Behavioral Task

We utilized a previously established sleep-dependent episodic memory task ([Figure 1A](#)), where subjects had to learn word-nonsense word pairs ([Mander et al., 2013](#)). In brief, words were 3-8 letters in length and drawn from a normative set of English words, while nonsense words were 6-14 letters in length and derived from groups of common phonemes. During encoding, subjects learned 120 word-nonsense pairs. Each pair was presented for 5 s. Participants performed the criterion training immediately after encoding. The word was presented along with the previously learned nonsense word and two new nonsense words. Subjects had to choose the correctly associated nonsense words and received feedback afterward. Incorrect trials were repeated after a variable interval, and were presented with two additional new nonsense words to avoid repetition of incorrect nonsense words. Criterion training continued until correct responses were observed for all trials.

During recognition, a probe word or a new (foil) probe word was presented along with 4 options: (1) the originally paired nonsense word, (2) a previously displayed nonsense word, which was linked to a different probe (lure), (3) a new nonsense word or (4) an option to indicate that the probe is new. During the recognition test after a short delay (10 min), 30 probe and 15 foil trials were presented. At

the long delay (10 h), 90 probe and 45 foil trials were tested. All probe words were presented only once during recognition testing, either during short or long delay testing.

Sleep Monitoring and EEG Data Acquisition

Polysomnography (PSG) sleep monitoring was recorded on a Grass Technologies Comet XL system (Astro-Med), including 19-channel electroencephalography (EEG) placed using the standard 10-20 system as well as Electromyography (EMG). Electrooculogram (EOG) was recorded the right and left outer canthi. EEG recordings were referenced to bilateral linked mastoids and digitized at 400 Hz in the range from 0.1 – 100 Hz. Sleep scoring was performed according to standard criteria in 30 s epochs (Rechtschaffen and Kales, 1968) (see Table S2 for sleep stage metrics for each group). Slow wave sleep (SWS) was defined as NREM stages 3-4, while NREM sleep encompassed stages 2-4. Given that stage 2 does not always exhibit pronounced SO activity (Figures 1C and 1D), we focused on SWS for all correlational analyses.

MRI Data Acquisition

Scanning was performed on a Siemens Trio 3T scanner with a 32-channel head coil. We obtained two high-resolution T1-weighted anatomical images, which were acquired using a three-dimensional MPRAGE protocol with the following parameters: repetition time, 1900 ms; echo time, 2.52 ms; flip angle, 9°; field of view, 256 mm; matrix, 256 × 256; slice thickness, 1.0 mm; 176 slices. MPRAGE images were co-registered, and the mean image was used to perform optimized voxel-based morphometry (VBM) to examine gray matter volume within specified regions of interest (ROI) as described below.

QUANTIFICATION AND STATISTICAL ANALYSIS

Behavioral Data Analysis

Memory recognition was calculated by subtracting both the false alarm rate (proportion of foil words, which subjects' reported as previously encountered) and the lure rate (proportion of words that were paired with a familiar, but incorrect nonsense word) from the hit rate (correctly paired word-nonsense word pairs). Memory retention was subsequently calculated as the difference between recognition at long minus short delays.

EEG Data

Preprocessing: EEG data were imported into EEGLAB and epoched into 5 s bins, which were visually inspected for artifacts. Then the continuous data was exported to FieldTrip for further analyses.

Spectral Analysis

(1) To obtain the average power spectra (Figure 1B), the raw data was epoched into non-overlapping 15 s segments and epochs containing artifacts were rejected. Data was tapered with a Hanning window and spectral estimates were calculated from 0.5 to 50 Hz in 0.5 Hz steps and averaged per subject and channel for all epochs in NREM sleep. (2) To obtain a continuous time-frequency representation of a whole night of sleep (Figures 1C and 1D), we utilized multitaper spectral analyses (Mitra and Pesaran, 1999; Pre-[rau et al., 2017](#)), based on discrete prolate spheroidal sequences. The raw data was epoched into 30 s long segments, with 85% overlap. Spectral estimates were obtained between 0.5 and 30 Hz in 0.5 Hz steps. We utilized 29 tapers, providing a frequency smoothing of ± 0.5 Hz.

Event Detection

Event detection (Figures 1D, 2A, and 2C) was performed for every channel separately based on previously established algorithms (Mölle et al., 2011; Staresina et al., 2015). (1) Slow oscillations: In brief, we first filtered the continuous signal between 0.16 and 1.25 Hz and detected all the zero crossings. Then events were selected based on time (0.8 – 2 s duration) and amplitude (75% percentile) criteria. Finally, we extracted artifact-free 5 s long segments (± 2.5 s around trough) from the raw signal. (2) Sleep spindles: We filtered the signal between 12-16 Hz and extracted the analytical amplitude after applying a Hilbert transform. We smoothed the amplitude with a 200 ms moving average. Then the amplitude was thresholded at the 75% percentile (amplitude criterion) and only events that exceeded the threshold for 0.5 to 3 s (time criterion) were accepted. Artifact-free events were then defined as 5 s long sleep-spindle epochs (± 2.5 s), peak-locked. Given that we observed prominent power differences between young and older adults (Figure 1B), we normalized events per subjects by means of a z-score prior to all subsequent analyses, unless stated otherwise (Figure 2A). The mean and standard deviation were derived from the unfiltered event-locked average time course of either SO or spindle events (e.g., Figures 1C and 1D, lower right) in every participants. Z-scores were then computed for all trials and time points.

Event-Locked Spectral Analysis

Time-frequency representations for artifact-free normalized SO (Figure 2B) were calculated after applying a 500 ms Hanning window. Spectral estimates (0.5 - 30 Hz; 0.5 Hz steps) were calculated between -2 and 2 s in steps of 50 ms and baseline-corrected by means of z-score relative to a bootstrapped baseline distribution that was created from all trials (baseline epoch -2 to -1.5 s, 10000 iterations; Flinker et al., 2015).

Event-Locked Cross-Frequency Coupling

For event-locked cross-frequency analyses (Dvorak and Fenton, 2014; Staresina et al., 2015), we first filtered the normalized SO trough-locked data (Figures 2D and 2E; spindle-locked in Figures 1C and 1D) into the SO component (0.1 - 1.25 Hz) and extracted

the instantaneous phase angle after applying a Hilbert transform. Then we filtered the same trials between 12–16 Hz and extracted the instantaneous amplitude from the Hilbert transform. We only considered the time range from -2 to 2 s to avoid filter edge artifacts. For every subject, channel, and epoch, we now detected the maximal sleep spindle amplitude and corresponding SO phase angle. The mean circular direction and resultant vector length across all NREM events were determined using the CircStat toolbox. In addition, we divided the SO phase into 17 linearly spaced bins and calculated the mean sleep spindle amplitude per bin. We normalized the individual sleep spindle amplitude distribution by the mean across all bins.

Data-Driven Cross-Frequency Coupling

We calculated a comodulogram on 15 s artifact-free long non-overlapping z-normalized segments during NREM sleep. We calculated the modulation index (Canolty et al., 2006) between lower (0.5 – 6.5 Hz; 0.5 Hz steps) and faster frequencies (8–40 Hz; 1 Hz steps). For the low frequency, we utilized a window of ± 1 Hz, which was adjusted for the lowest frequencies. For faster frequencies, the window was adjusted to capture the side peaks. Hence, the window at a given frequency was always defined as the low center frequency + 1 Hz, i.e., at 15 Hz, the window to assess coupling to the 3 Hz phase was ± 4 Hz; while at 5 Hz the window was ± 6 Hz. The modulation index was normalized by a bootstrapped z-score relative to a distribution that was obtained by random-point block-swapping (200 iterations).

Cross-Frequency Directionality Analysis

To determine whether low frequencies components drive sleep spindle activity during SWS or vice versa, we calculated the cross-frequency phase slope index (Jiang et al., 2015; Helfrich et al., 2017) between the normalized signal and the signal filtered in the sleep spindle range (12–16 Hz). To avoid edge artifacts, we restricted this analysis to ± 2 seconds around the SO trough. Hence, these 4 s long segments include at least 3 cycles of the SO oscillation (~ 0.75 Hz), in accordance with previous reports (Jiang et al., 2015). We considered frequencies between 0.5 and 4 Hz (0.5 Hz steps; 0.25 Hz bandwidth) after applying a Hanning window and extracting the complex Fourier coefficients. Significant values above zero indicate that SO drive sleep spindle activity, while negative values indicate that sleep spindles drive SO. Values around zero indicate no directional coupling. We repeated this analysis based on 15 s long segments, which were then averaged across all available NREM events to demonstrate that the findings are not confounded by the chosen window length (Figure S2D).

Detection of SO and Spindle Frequency Peaks

(1) SO peak frequency (related to Figure 1B): In order to disentangle the true oscillatory SO component from the prominent $1/f$ slope, we utilized irregular-resampling auto-spectral analysis (IRASA; Wen and Liu, 2016). We analyzed non-overlapping 15 s segments of continuous artifact-free data during NREM sleep and assessed frequencies between 0.1 and 30 Hz. IRASA takes advantage of the fact that irregularly resampling of the neuronal signals by pairwise non-integer values (resampling factor rf and corresponding factor rf^* : e.g., 1.1 and 0.9) slightly shifts the peak frequency of oscillatory signals by compressing or stretching the underlying signal. However, the $1/f$ component remains stable. This procedure is then repeated in small, overlapping windows (window size: 5 s, sliding steps: 1 s; resampling factors rf : 1.1–1.9 in 0.05 increments). Note resampling was always done in a pairwise fashion for factor h and the corresponding resampling factor $rf^* = 2 - rf$. For each segment, we calculated the auto-power spectrum by means of a FFT after applying a Hanning window. Then all auto-spectra were median-averaged to obtain the power spectrum of the $1/f$ component, with the idea being that resampled oscillatory components are averaged out. Finally, the resampled $1/f$ PSD is subtracted from the original PSD to obtain the oscillatory residuals on which we performed the individual peak detection (SO range: peak < 2 Hz; spindle-range: 9–17 Hz).

(2) In addition to IRASA, which provides a mean sleep spindle peak frequency, we also utilized a linear de-trending approach to assess spindle frequencies as a function of the SO phase (Figure 3C), where we investigated whether SO modulates additional sleep spindle features besides the amplitude on a fine-grained temporal scale. Therefore, we screened every artifact-free normalized SO event (-1.25 to 1.25 around trough) at every channel separately for oscillatory activity in the sleep spindle range. First, we zero-padded every trial to 10 s to increase the frequency resolution (0.1 Hz), then applied a Hanning window and obtained spectral estimates between 8 and 16 Hz. The resulting power values were log transformed. The sleep spindle peak for every SO was detected after subtraction of linear fit to the spectrum to remove the $1/f$ component. Second, every trial was filtered at the trial-specific peak frequency (± 2 Hz) and the instantaneous amplitude was extracted from a Hilbert transform before we performed event-related cross-frequency coupling analyses. In addition, we only considered SO that contained sleep spindle events that exceeded the 75% percentile of sleep spindle amplitudes to ensure comparability for correlation analyses. This approach effectively corrected for differences in sleep spindle peak frequencies and spectral power distributions prior to correlation with behavior. To obtain time-resolved sleep spindle peak frequency estimates, we detected the sleep spindle peak as described above in a 500 ms sliding window approach. We shifted the window in 25ms steps relative to the SO events (-1 to 1 s; ± 250 ms) and recalculated the sleep spindle peak frequency. Finally, we smoothed the resulting traces with a 100ms moving average.

Structural MRI Data Analysis

To measure gray matter volume, optimized voxel-based morphometry (VBM) was performed using SPM8 (Penny et al., 2011) (Wellcome Department of Imaging Neuroscience) with the VBM8 toolbox (<http://dbm.neuro.uni-jena.de/vbm.html>) and the Diffeomorphic Anatomical Registration through Exponentiated Lie algebra (DARTEL) toolbox in order to improve registration of older brains to the normalized MNI template (Mak et al., 2011; Mander et al., 2013). To enhance signal to noise ratio, two T1-weighted MPRAGE images were first co-registered and averaged. Averaged images were then segmented applying the Markov random field approach

(Rajapakse et al., 1997) and then registered, normalized, and modulated using DARTEL. Grey matter and white matter segmentations were inputted into DARTEL and utilized to create a study specific template, which was then used to normalize individual brains into MNI space. Modulated gray matter maps were then smoothed using an 8 mm Gaussian kernel.

Measures of total intracranial volume (TIV) for each participant were estimated from the sum of gray matter, white matter, and CSF segmentation, and then used to adjust gray matter volumetric measures to account for differences in head size. Given that slow oscillations, sleep spindles, and ripples depend on the interaction between prefrontal cortex, thalamus, and hippocampus regions, the Anatomical Automatic Labeling repository (Tzourio-Mazoyer et al., 2002) within the Wake Forest University PickAtlas toolbox (Maldjian et al., 2003) was used to generate anatomically-based ROIs for the hippocampus, thalamus, medial prefrontal cortex, and orbitofrontal cortex, as well as all other control ROIs. Mean voxelwise gray matter volume within anatomically defined ROIs were extracted using the Marsbar toolbox (Brett et al., 2002) and used in analyses relating gray matter volumetric measures with sleep and memory variables.

Statistical Analysis

Unless stated otherwise, we used cluster-based permutation tests (Maris and Oostenveld, 2007) to correct for multiple comparisons as implemented in FieldTrip (Monte Carlo method; 1000 iterations; maxsize criterion). Clusters were formed in time/frequency (e.g., Figures 2B and 2F) or space (e.g., Figures 2E and 2G) by thresholding independent t tests (e.g., Figures 2E–2G), circular-linear (e.g., Figures 3A and 3D) or linear correlations (Spearman, e.g., Figure 4A) at $p < 0.05$. Correlation values were transformed into t-values. A permutation distribution was then created by randomly shuffling labels. The permutation p value was obtained by comparing the cluster statistic to the random permutation distribution. The clusters were considered significant at $p < 0.05$ (two-sided). Bonferroni-correction was applied to correct for multiple cluster tests (e.g., Figure 4B).

Circular statistics were calculated using the CircStat toolbox. Circular non-uniformity was assessed with Rayleigh tests at $p < 0.01$. Effect sizes were quantified by means of Cohen's d, the correlation coefficient rho or η^2 in case of repeated-measures ANOVAs or Watson-Williams-tests (circular ANOVA equivalent). Circular-linear correlations were calculated according to the following formula:

$$\rho = \sqrt{\frac{r_{XS}^2 + r_{XC}^2 - 2 * r_{XS} * r_{XC} * r_{CS}}{1 - r_{CS}^2}}$$

where r_{XS} , r_{XC} and r_{CS} were defined as

$$r_{XS} = \text{corr}(x, \sin(\alpha))$$

$$r_{XC} = \text{corr}(x, \cos(\alpha))$$

$$r_{CS} = \text{corr}(\sin(\alpha), \cos(\alpha))$$

with x being the linear and alpha being the circular variable. In order to control for confounding variables, we utilized partial correlations, where c was partialled out of x, sin(alpha) and cos(alpha) before computing the multiple correlation using the regression residuals. We utilized a threshold of 10% to define clusters following partial correlations, which were then again tested at a cluster alpha of 0.05 (Maris and Oostenveld, 2007). To obtain effect sizes for cluster tests, we calculated the effect size separately for all channel, frequency and/or time points and averaged across all data points in the cluster. Repeated-measures ANOVAs were Greenhouse-Geisser corrected.

DATA AND SOFTWARE AVAILABILITY

Freely available software and algorithms used for analysis are listed in the [Key Resources Table](#). All custom scripts and data contained in this manuscript are available upon request from the Lead Contact.

Neuron, Volume 97

Supplemental Information

Old Brains Come Uncoupled in Sleep:

Slow Wave-Spindle Synchrony,

Brain Atrophy, and Forgetting

Randolph F. Helfrich, Bryce A. Mander, William J. Jagust, Robert T. Knight, and Matthew P. Walker

Supplemental Information

Table S1 related to Figure 1A and Results
Demographic and Neuropsychological Measures (mean \pm SD)

Variable	Young ($n = 20$)	Older ($n = 32$)
Age (yr)	20.4 \pm 2.0	73.8 \pm 5.3***
Sex	12 Female	22 Female
Mean prestudy bed time	0:20 \pm 0:53	22:50 \pm 1:14***
Mean prestudy wake time	8:27 \pm 0:52	7:14 \pm 1:11***
Mean prestudy time in bed (hr)	8.11 \pm 0.58	8.39 \pm 0.74
Mean prestudy sleep time (hr)	7.75 \pm 0.61	7.13 \pm 0.95*
Mean prestudy sleep latency (min)	15.7 \pm 9.2	34.9 \pm 41.7*
Mean prestudy sleep efficiency (%)	95.6 \pm 3.4	85.3 \pm 11.3***
MMSE	29.6 \pm 0.9	29.4 \pm 0.9
<i>Neuropsychological Measures</i>		
CVLT (long delay, # free recalled)		11.1 \pm 3.0
WMS (visual reproduction %)		75.0 \pm 16.8
Trailmaking B (seconds)		72.8 \pm 34.1
Stroop (# correct in 60 seconds)		50.1 \pm 14.0

*denotes $P < 0.05$, ** $P < 0.01$, *** $P < 0.001$

Table S2 related to Figure 1C/D and Results
Sleep statistics (mean \pm SE)

Variable	Young (<i>n</i> = 20)	Older (<i>n</i> = 32)
Total Recording Time (min)	480.4 \pm 0.2	479.5 \pm 0.6
Total Sleep Time (min)	431.6 \pm 6.1	340.3 \pm 11.8***
Sleep Latency (min)	16.6 \pm 2.8	22.4 \pm 4.6
Wake After Sleep Onset	27.9 \pm 5.8	115.1 \pm 10.9***
Stage 1 (min)	14.3 \pm 1.6	22.3 \pm 1.4***
Stage 2 (min)	201.1 \pm 6.7	192.6 \pm 10.0
Slow Wave Sleep (min)	117.9 \pm 7.1	60.9 \pm 6.4***
Rapid Eye Movement Sleep (min)	98.3 \pm 6.1	64.4 \pm 5.4***
Sleep Efficiency (%)	90.8 \pm 1.3	71.3 \pm 2.5***

*denotes $P < 0.05$, ** $P < 0.01$, *** $P < 0.001$

Table S3 related to Figure 3A and Results
Learning, bedtime and retrieval time

Variable	Young (<i>n</i> = 20)	Older (<i>n</i> = 32)
Encoding time	19:30h ± 41min	19:10h ± 56min
Encoding to bedtime (min)	4.03h ± 40min	3:23h ± 36min
Duration of criterion training (min)	27:39 ± 4:03min	39:09 ± 11.27min
Immediate test time	20:17h ± 39min	20:03h ± 1:04h
Wake time	7:31h ± 30min	6:34h ± 1:06h
Wake to retrieval time (min)	2:31h ± 55min	2:19h ± 40min

Table S4 related to Figure 3C/D
Individual SO and spindle features (mean \pm SEM)

Event type and feature	Young (n = 20)	Older (n = 32)
SO		
Number of events [N]	4350 \pm 113	3263 \pm 162***
Duration [s]	1.11 \pm 0.01	1.12 \pm 0.01
Amplitude uncorrected [μ V]	109.19 \pm 5.52	49.35 \pm 2.10***
Amplitude normalized [z]	5.46 \pm 0.06	5.65 \pm 0.11
Frequency [Hz]	0.80 \pm 0.03	0.71 \pm 0.04
Spindles		
Number of events [N]	3391 \pm 132	1636 \pm 127***
Duration [s]	0.87 \pm 0.02	0.71 \pm 0.01***
Amplitude uncorrected [μ V]	45.44 \pm 2.68	27.44 \pm 2.76***
Amplitude normalized [z]	12.51 \pm 0.5	17.95 \pm 2.94
Frequency [Hz]	12.58 \pm 0.17	11.75 \pm 0.11***

*denotes $P < 0.05$, ** $P < 0.01$, *** $P < 0.001$

Number of detected events in NREM sleep at electrode Fz. Average median event duration. Peak-to-peak amplitude uncorrected and after z-normalization (see also **Figure 2A**). Note that z-normalization corrected for the pronounced SO amplitude differences (uncorrected: $p < 0.0001$; normalized: $p = 0.1968$) as well as for pronounced spindle power differences (uncorrected: $p < 0.0001$; normalized: $p = 0.1536$). We corrected for differences in the total number of spindle events by bootstrapping coupled events (**Figure S1G/H**). We accounted for differences in event duration by a stratification approach (**Figure S1D-F**) and corrected for differences in spindle peak frequencies by filtering in individual frequency bands (**Figure 3C/D and Figure S3**).

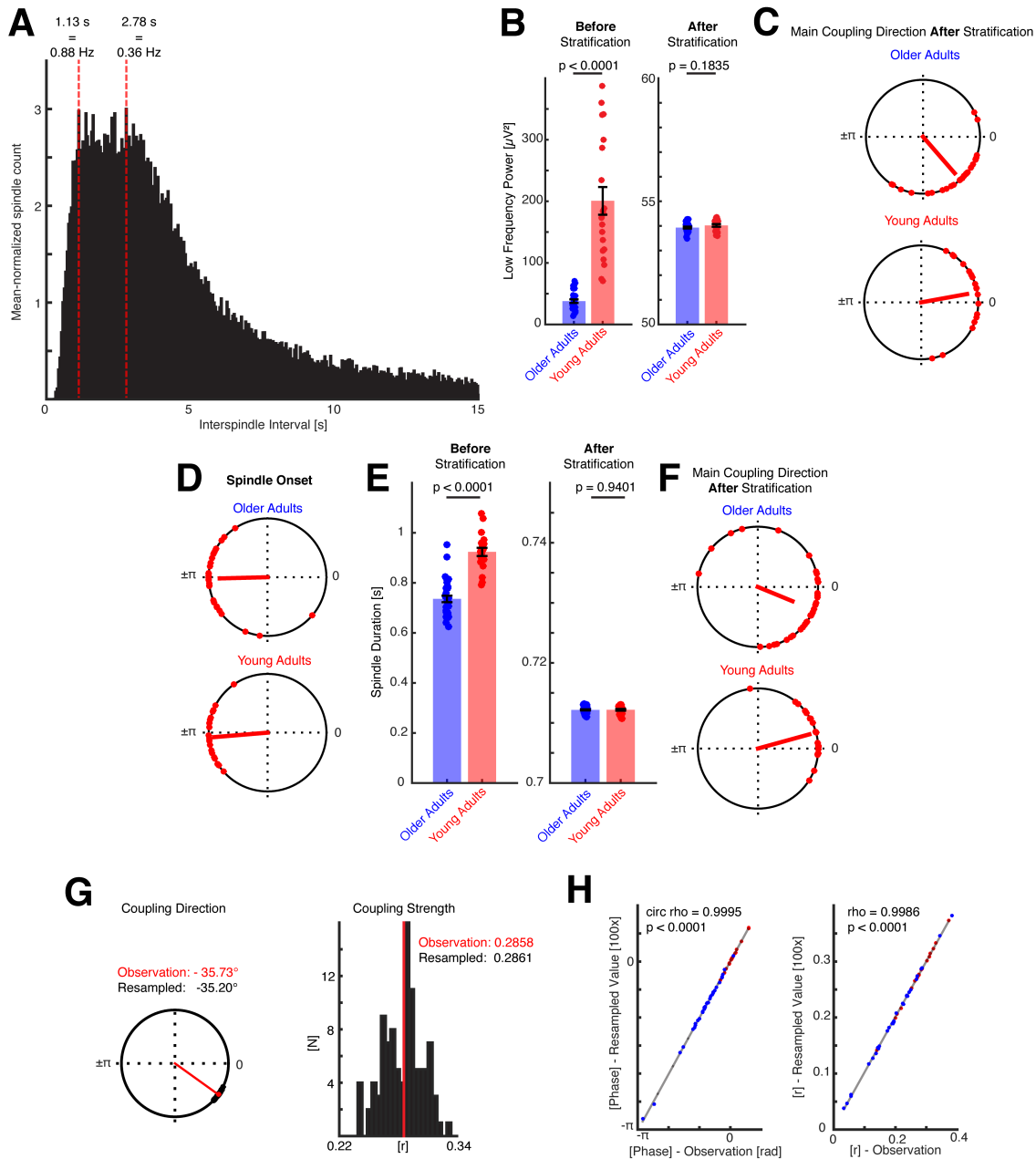
Table S5 related to Figure 3A
Partial circular-linear correlation results

	rho	p value
Original observation (Figure 3A)	0.57	0.0004***
Factors partialled out:		
Age	0.37	0.0366*
Mean prestudy bed time	0.45	0.0074**
Mean prestudy wake time	0.47	0.0055**
Mean prestudy time in bed (hr)	0.60	0.0002***
Mean prestudy sleep time (hr)	0.57	0.0005***
Mean prestudy sleep latency (min)	0.55	0.0007***
Mean prestudy sleep efficiency (%)	0.54	0.0009***
MMSE	0.57	0.0004***
Total Recording Time (min)	0.54	0.0008***
Total Sleep Time (min)	0.53	0.0013**
Sleep Latency (min)	0.57	0.0004***
Wake After Sleep Onset	0.52	0.0015**
Stage 1 (min)	0.54	0.0009***
Stage 2 (min)	0.58	0.0003***
Slow Wave Sleep (min)	0.57	0.0004***
Rapid Eye Movement Sleep (min)	0.56	0.0006***
Sleep Efficiency (%)	0.53	0.0012**

*denotes $P < 0.05$, ** $P < 0.01$, *** $P < 0.001$

In order to account for the differences in various sleep parameters (**Table S1 and S2**) on the group differences in memory retention, we partialled out the confounding linear variables from the circular-linear correlations. We found that the relationship between coupling phase and behavior remained unchanged. Thus, differences in sleep architecture do not significantly contribute to the observed differences in memory retention.

Figure S1 related to Figure 1C/D and 2A/C/D/E



SO-spindle coupling features and control analyses

(a) Histogram of normalized mean inter-spindle intervals. A Poisson process implies that the inter-event interval grows exponentially. However, sleep spindles exhibit a non-Poisson like distribution. Sleep spindle expression and/or generation, just like single neurons, exhibits refractory periods and rhythmic modulations, which might arise from endogenous network dynamics. The histogram indicates that two detected sleep spindle events never immediately followed each other (values below 0.225 seconds are 0). We detected the first two maxima of the distribution (at 1.13 and 2.78 seconds), which is in accordance with a rhythmic modulation by a < 1 Hz process, where subsequent sleep spindles are separated by 1-3 SO cycles. Note the majority of events during NREM sleep was detected in the range < 5 seconds. Individual distributions were mean normalized to account for differences in absolute event numbers

between subjects. In accordance with this finding that SO peak frequencies were below 1 Hz, and did not differ between subject groups (see also **Table S4**).

(b) Stratification of power differences. Left: We observed prominent low frequency (<4 Hz) power differences before stratification (electrode Cz; $t_{50} = -9.00$, $p < 0.0001$, $d = 2.26$). Right: We utilized a FFT to transform the SO trough-locked raw time series into the frequency domain and then stratified the power distributions between old and young subjects based on 1000 bins and 10000 iterations. This approach effectively removed all power differences between groups ($t_{50} = -1.35$, $p = 0.1835$, $d = 0.38$; right side). However, this approach removed as much as 98.9% of all trials in some subjects, given the pronounced power differences (left panel; note the differences in scaling of the y-axis).

(c) We then repeated the event-locked cross-frequency coupling analyses. We found significant non-uniform distributions in both, older (Rayleigh $z = 23.01$, $p < 0.0001$) and younger adults (Rayleigh $z = 13.33$, $p < 0.0001$), which differed significantly (Watson-Williams test: $F_{1,50} = 34.65$; $p < 0.0001$; $\eta^2 = 0.38$) and confirmed the main coupling direction results (**Figure 2D**; older adults: $-49.1^\circ \pm 31.6^\circ$; young adults: $10.3^\circ \pm 34.7^\circ$; circular mean \pm SD).

(d) Spindle onset and duration analyses. We tested whether differences in sleep spindle onsets or duration could explain any of the observed coupling differences (electrode Cz). We first detected the spindle onset per subject based on their average spindle waveform. We first band-pass filtered the spindle-locked average in the range from 12-16 Hz and normalized it by a z-score. We then detected all the peaks and defined the onset of the spindle as the first peak that exceeded 5% of the largest peak. Following this we extracted the corresponding SO phase from the Hilbert transform. We found that spindles started around the SO 'down-state' in both old and young adults (older adults: Rayleigh $z = 21.2$, $p < 0.0001$; $-178.5^\circ \pm 35.0^\circ$; younger adults: Rayleigh $z = 16.62$, $p < 0.0001$; $-175.2^\circ \pm 24.1^\circ$; circular mean \pm SD). The onset did not differ between older and younger adults (Watson-Williams test: $F_{1,50} = 0.13$, $p = 0.7205$, $\eta^2 = 0.002$).

(e) To address spindle duration differences between groups, we defined the spindle duration as the time that the individual spindle exceeded detection threshold. The analysis was based on the individual spindle peak frequencies (**Table S4**). Left: Spindles were of a significantly longer duration in younger adults ($t_{50} = -6.64$, $p < 0.0001$, $d = 1.86$); a finding that may explain why spindles peak significantly later in the SO cycle relative to older adults. Right: We then stratified the old and young groups based on the spindle duration (50 bins, 10000 repetitions) until no significant group differences were detected ($t_{50} = -0.08$, $p = 0.9401$, $d = 0.02$).

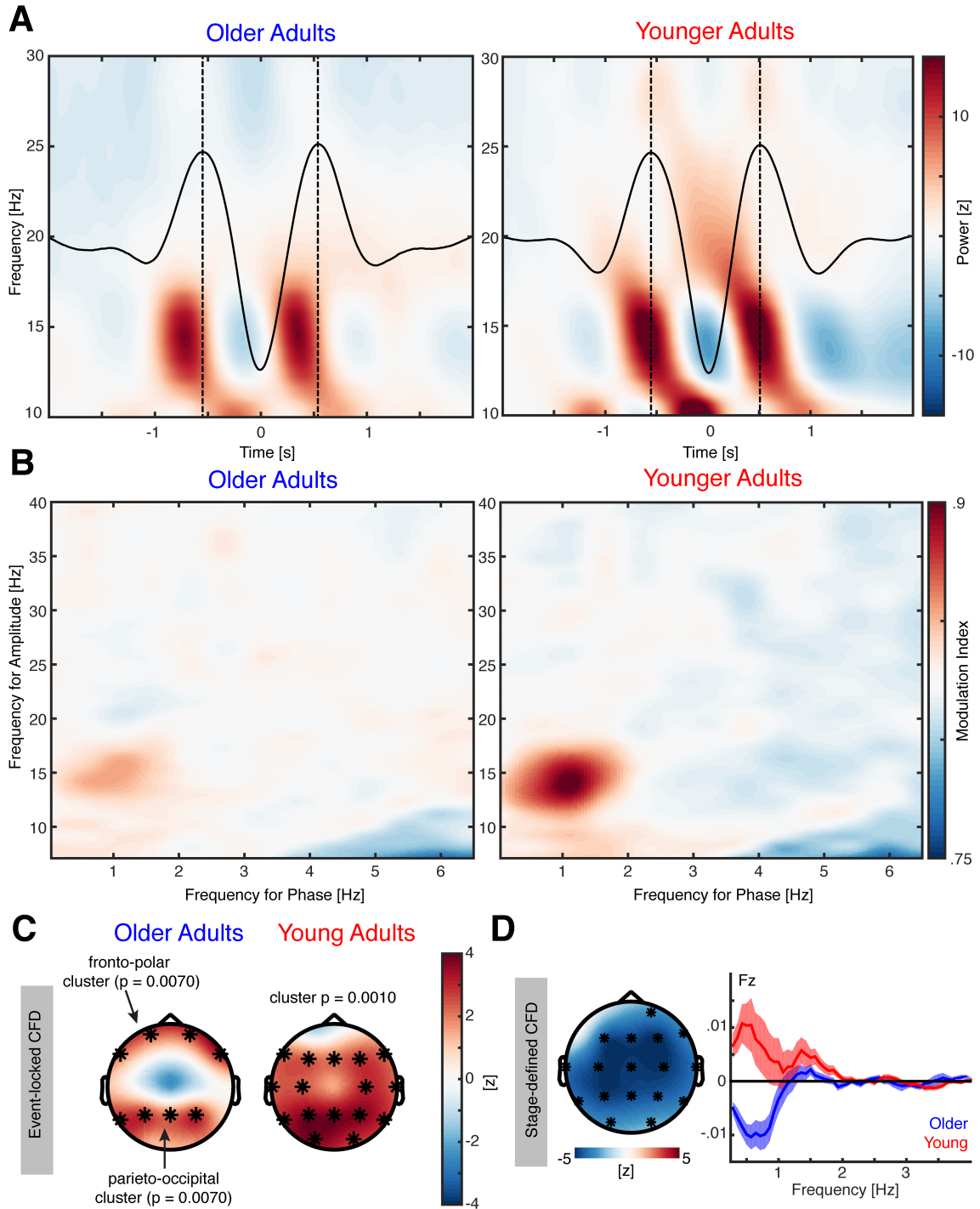
(f) We repeated the event-locked cross-frequency coupling analyses based on the stratified distributions and again observed significant non-uniform distributions in both, older (Rayleigh $z = 12.44$, $p < 0.0001$) and younger adults (Rayleigh $z = 15.67$, $p < 0.0001$). The groups differed significantly (Watson-Williams test: $F_{1,50} = 8.30$; $p = 0.0058$; $\eta^2 = 0.12$), confirming the main coupling direction results (older adults: $-22.4^\circ \pm 49.7^\circ$; young adults: $15.4^\circ \pm 27.4^\circ$; circular mean \pm SD).

(g) Bootstrapped coupling estimates account for different event counts. Coupling estimates are easily distorted by differences in amplitude and event numbers. Younger adults exhibited more detected SO during NREM sleep than older adults ($t_{50} = -4.7804$, $p < 0.0001$, $d = 1.46$; **Table S4**). Here we normalized all time series prior to subsequent analyses. In order to control for differences in event numbers, we employed a random resampling approach. On 100 iterations, we recalculated the coupling strength and direction for 1000 randomly sampled SO events and found that the result remained unchanged (resultant vector length: Spearman $\rho = 0.9986$, $p < 0.0001$; average deviation: -0.0008 ± 0.0020 ; coupling direction: circular-circular $\rho = 0.9995$, $p < 0.0001$; average circular deviation $-0.11^\circ \pm 0.96^\circ$; mean \pm SD). Thus, differences in event numbers were statistically unlikely to explain the reported group differences, with sufficient number of events detected in each group to reliably estimate cross-frequency coupling in an unbiased manner. Single subject example. Data from one representative older adult is displayed. Left: black dots indicate 100 resampled mean directions, while the red line indicates the observed direction when all available events ($n = 3733$) were considered. The deviation observed deviation

was less than 1° . Right: Distribution of resampled resultant vector length (black) and the observed (red) value. Again, the deviation was negligible (< 0.01).

(h) Left: Circular-circular correlation between the observed and bootstrapped coupling direction. The mean deviation was $-0.11^\circ \pm 0.96^\circ$ (circular mean \pm SD) and the correlation was nearly 1. This indicates that every participant exhibited a sufficient number of events to reliably estimate the mean coupling direction and strength. Therefore, differences in event number are negligible and did not alter the results. Right: Linear correlation between observed coupling strength and resampled coupling strength. The average deviation was -0.0008 ± 0.0020 (mean \pm SD) and the correlation approached 1.

Figure S2 related to Figure 2B/C/F/G



Grand-average spectrograms, comodulograms and directionality analyses

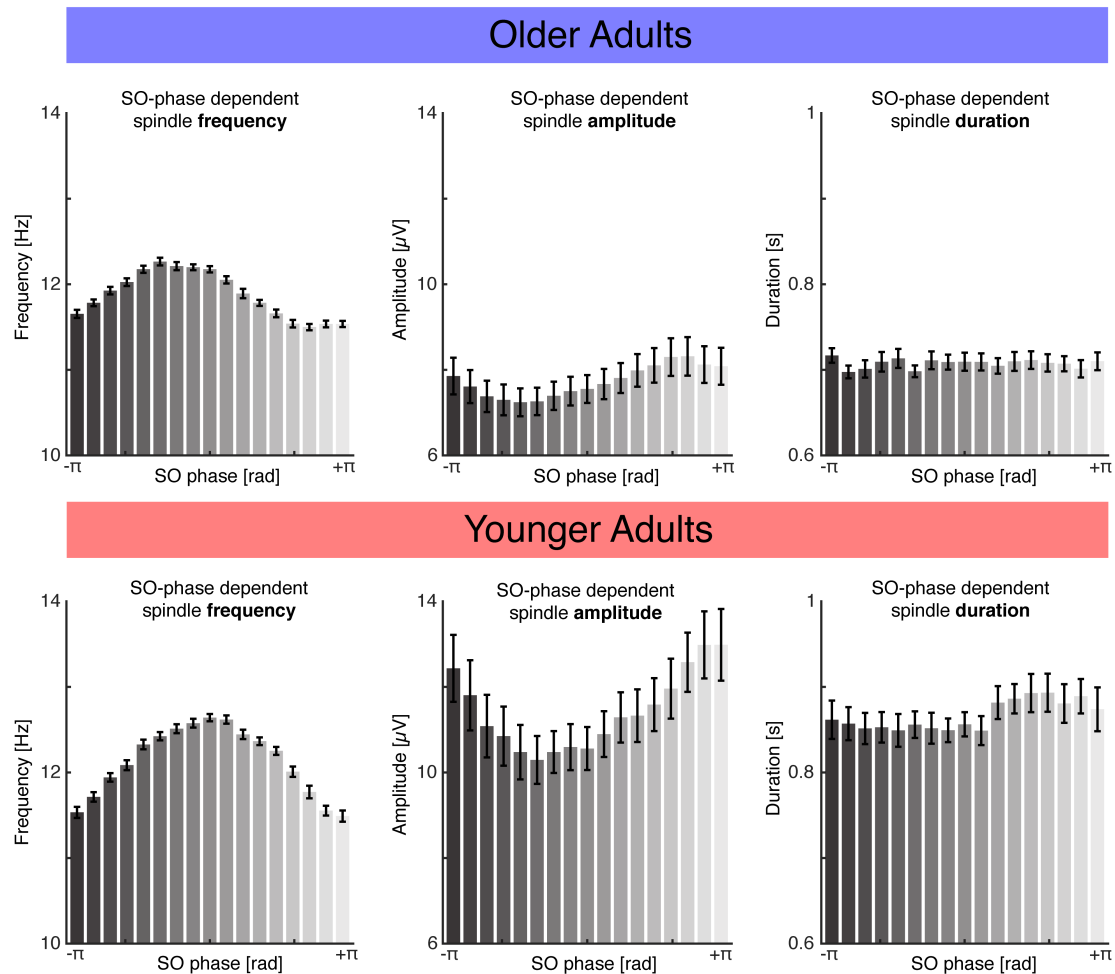
(a) Baseline-corrected grand-average SO-locked time-frequency representations underlying **Figure 2B** for older (left) and young (right) participants. The normalized and rescaled corresponding average SO event is superimposed in black. Dashed black lines depict the two largest SO peaks. Note that activity in sleep spindle range (12-16 Hz) peaks before the dashed line in older adults, while their occurrence coincides in younger adults.

(b) Grand-average normalized comodulogram underlying **Figure 2F** for older (left) and young (right) adults. Note the strongest effect was observed in the SO-spindle range in both older and young adults, but the magnitude was increased in young adults.

(c) Directional SO-Spindle Cross-Frequency Coupling. We assessed whether SO predicted spindle activity separately for young and older adults. Therefore, we tested the PSI at every electrode against zero. We found that older adults exhibited two clusters, one fronto-polar ($p = 0.0070$, $d = 0.75$) and one over parieto-occipital sensors ($p = 0.0070$, $d = 0.73$). Crucially, directional SO-spindle influences were attenuated over fronto-central sensors. Young adults only exhibited one large widespread significant cluster, indicating the SO mediated sleep spindle timing in multiple cortical regions ($p = 0.0010$, $d = 1.05$). Note that this cluster overlapped with the anterior cluster in older adults in two electrodes (F7/8), but not at electrodes Fp1 and Fp2 (anterior electrodes). This was due to increased variance at electrodes Fp1/2 in younger adults caused by one outlier value (SD older adults: 0.0091; SD younger adults: 0.1092). After removal of that subject, PSI values were also above zero in younger adults (0.0034 ± 0.0149 ; mean \pm SD; though not significantly different from zero, $t_{18} = 1.01$, $p = 0.3277$, $d = 0.33$).

(d) We assessed the cross-frequency directional coupling (CFD) in an event-like character, centered on detected SOs (± 2 seconds; **Figure 2G** and **Figure S2C**). Four seconds is sufficient to capture 3 cycles of the low frequency component (SO peak frequency ~ 0.75 Hz; see also **Table S4**). We also repeated the analysis based on a continuous 15 second segments (see **Figure 1B**) during NREM sleep to rule out that the 4 second signal length confounded PSI estimates. We again observed that SO-spindle directional cross-frequency coupling was reduced in older as compared to younger adults (left; $p = 0.001$; $d = 1.26$). The main differences were observed in < 1 Hz range (right panel). This result confirmed that SO drive spindle activity in younger adults and that this is reduced in older adults.

Figure S3 related to Figure 3C



SO phase dependent spindle features

Summary of SO-dependent spindle features in NREM sleep (electrode Fz).

Left column: Spindle frequency as a function of the SO phase (related to **Figure 3C**).

Center column: SO-phase dependent spindle amplitudes were determined after testing if individual SO events contained an oscillatory component in the spindle range (peak in the linearly de-trended power spectrum to correct for the $1/f$ bias). Note that this approach also captures spindle activity that would remain below detection threshold, using traditional spindle event detectors (amplitude criterion). Here we observed that older and younger adults have similar spindle amplitude distributions relative to the SO phase. While the overall power is reduced in older adults, the distributions are similar with overall higher values observed between 0 and $+\pi$ (SO peak to trough = falling flank), while lower values were observed between $-\pi$ and 0 (SO trough to peak = rising flank). Therefore, the relative 75% percentile amplitude criterion skewed the frequency and amplitude distribution-corrected average coupling phase angles in **Figure 3D** towards values $> 0^\circ$.

Right column: Note that this approach based on detecting spindle signatures in SO biases the spindle duration towards short-lasting events, given the nesting within the SO cycle (event criterion: 0.8 to 2s). Therefore, we extracted the median duration per subject from the detected spindle events and then assessed the respective SO phase distribution.